REPORT DOCUMENTATION PAGE

Form Approved OMB NO. 0704-0188

1. REPORT DATE (DD-MM-YYYY)	2. REPORT TYPE	3. DATES COVERED (From - To)
08-06-2012	Final Report	12-Jun-2007 - 11-Jun-2011

4. TITLE AND SUBTITLE
The Integration of Nanoscale Techniques for an Improved Battery Technology

5a. CONTRACT NUMBER
W911NF-07-1-0398

5b. GRANT NUMBER

5c. PROGRAM ELEMENT NUMBER
106011

6. AUTHORS
Dale Teeters

5d. PROJECT NUMBER

5e. TASK NUMBER

5f. WORK UNIT NUMBER

7. PERFORMING ORGANIZATION NAMES AND ADDRESSES
University of Tulsa
Research & Sponsored Programs
The University of Tulsa
Tulsa, OK 74104 -3189

8. PERFORMING ORGANIZATION REPORT NUMBER

9. SPONSORING/MONITORING AGENCY NAME(S) AND ADDRESS(ES)
U.S. Army Research Office
P.O. Box 12211
Research Triangle Park, NC 27709-2211

10. SPONSOR/MONITOR'S ACRONYM(S)
ARO

11. SPONSOR/MONITOR'S REPORT NUMBER(S)
52445-CH-DPS.12

12. DISTRIBUTION AVAILIBILITY STATEMENT
Approved for Public Release; Distribution Unlimited

13. SUPPLEMENTARY NOTES
The views, opinions and/or findings contained in this report are those of the author(s) and should not contrued as an official Department of the Army position, policy or decision, unless so designated by other documentation.

14. ABSTRACT
Lithium batteries continue to receive much attention today because they offer a number of significant advantages. However, there are major problems that must be solved and advances that can be made for these battery systems, if they are to reach even higher performance. New advances in battery technology are needed so that the great advances associated with electronic devices such as computer systems, sensors, monitoring systems and other new devices of the future can continue to develop. Battery technology is complicated and there is room for

15. SUBJECT TERMS
Nanostructured electrodes, nanostructured electrolyte, 3-D battery architecture, integrated nanostructured battery

16. SECURITY CLASSIFICATION OF:			17. LIMITATION OF ABSTRACT	15. NUMBER OF PAGES	19a. NAME OF RESPONSIBLE PERSON
a. REPORT	b. ABSTRACT	c. THIS PAGE			Dale Teeters
UU	UU	UU	UU		19b. TELEPHONE NUMBER: 918-631-3147

Report Title

The Integration of Nanoscale Techniques for an Improved Battery Technology

ABSTRACT

Lithium batteries continue to receive much attention today because they offer a number of significant advantages. However, there are major problems that must be solved and advances that can be made for these battery systems, if they are to reach even higher performance. New advances in battery technology are needed so that the great advances associated with electronic devices such as computer systems, sensors, monitoring systems and other new devices of the future can continue to develop. Battery technology is complicated and there is room for improvement in many of the components that make up this power system. Specifically, improvements in the stabilization of the electrode/electrolyte interface (lithium metal batteries), in electrolyte performance and in cell geometry and cathode structure are needed for lithium batteries. Nanoscale science and engineering has the potential to be the mechanism for addressing the concern in all of these areas. The work described here involves the improvement of battery technology by addressing problems in the component parts of batteries by using an integrated nanotechnology approach.

Enter List of papers submitted or published that acknowledge ARO support from the start of the project to the date of this printing. List the papers, including journal references, in the following categories:

(a) Papers published in peer-reviewed journals (N/A for none)

Received Paper

TOTAL:

Number of Papers published in peer-reviewed journals:

(b) Papers published in non-peer-reviewed journals (N/A for none)

Received Paper

TOTAL:

Number of Papers published in non peer-reviewed journals:

(c) Presentations

Dale Teeters"Development and Commercialization of a Lithium Battery System," Invited Presentation, NanoFocus State Nanotech Conference, Oklahoma City, OK, January 2011.

Dale Teeters "Interfacial Storage of Lithium in the Nanostructure of SnO2 Nanobaskets for Capacities Exceeding Theoretical Values," International Meeting on Lithium Batteries, Montreal, Canada, June 2010.

D. Decker and D. Teeters, "Blooming of Wax Surfactants to the Surface of Polymer Electrolytes to Stabilize Passivation at the Lithium Electrode/Polymer Interface," International Meeting on Lithium Batteries, Montreal, CA, June 2010.

M. Smith, P. Johnson, D. Teeters, "Electrochemical Characterization of SnO2 Nanobasket Electrodes with Capacities Exceeding Theoretical Values," 55th Oklahoma Pentasectional Meeting of the American Chemical Society, Norman, OK April 10, 2010

Dale Teeters "Batteries on the Nanoscale: More Than Just a Power Supply," Invited Presentation, NanoFocus State Nanotech Conference, Midwest City, OK, April 2010.

Dale Teeters "Nanotechnology: What is it and Can It Power Our Society in the Future," Invited Presentation, Southwestern Oklahoma State University, April 2010.

Dale Teeters "Nanobatteries: Power Sources for Autonomous Miniaturized Systems," Invited Presentation, Department of Physics, The University of Tulsa, February 2010.

Dale Teeters "Powering Our Society for the Future: The Use of Nanotechnology to Improve Energy Storage," Invited Presentation, University of Central Oklahoma, February 2010.

M. Smith, S. Haheshwari, P. Johnson, D. Teeters, "Characterization of the Importance of Nanostructuring in SnO2 Nanobasket Electrode Materials," 17th International Conference on Solid State Ionics, Toronto, Canada, June 28, 2009.

C. Bishop and D. Teeters, "Conductivity of Poly(ethylene oxide)/Lithium Triflate in Thin Film Geometries," 17th International Conference on Solid State Ionics, Toronto, Canada, June 28, 2009.

P. Johnson, W. Collier, M. Smith, G. Strout, K. Roberts and D. Teeters, "Characterization of SnO2 Nanobasket Electrode Material," 17th International Conference on Solid State Ionics, Toronto, Canada, June 28, 2009.

Dale Teeters "Potential Battery Performance Using Nanotechnology," Invited Presentation, Frontier Electronic System, Stillwater, OK, June 8, 2009.

Dale Teeters "Nanobatteries: Power Sources for Autonomous Miniaturized Systems," Invited Speaker, New Energy Solutions in Tours (NEST) 2009: International Workshop, Tours, France, May 26-27, 2009

Dale Teeters "A 3-D Nanobattery System with Individually Wired Nano-electrodes for Enhanced Performance," Invited Presentation, 2009 NSTI Nanotechnology Conference and Trade Show, May 3-7, 2009, Houston, Texas, U.S.A

C. Bishop and D. Teeters, "Thermal and Conductive Characteristics of a Nano-confined PEO/Lithium Triflate Complex," 54th Pentasectional Meeting of the Oklahoma Sections of the American Chemical Society, Oral Roberts University, Tulsa, April 18, 2009.

Dale Teeters "Enhanced Battery Performance Using a 3-D Nanobattery Architecture with Individually Wired Nano-electrodes, 54th Pentasectional Meeting of the Oklahoma Sections of the American Chemical Society, Oral Roberts University, Tulsa, April 18, 2009.

Dale Teeters "Individually-wired nanoelectrodes for a 3-D nanostructured battery systems," 237th ACS National Meeting, Salt Lake City, UT, March 22-26, 2009

D. Kordonowy, C. Smith; D. Teeters, "Ion concentrations at the surfaces of poly(ethylene oxide) films related to the casting substrate's surface free energy," 237th ACS National Meeting, Salt Lake City, UT, United States, March 22-26, 2009

Dale Teeters "Nanotechnology: What is It and Can it Power Our Society in the Future," D. Teeters, Invited Speaker, Northeastern Oklahoma State University, Tahlequah, OK, February 11, 2009.

Dale Teeters “Nanotechnology: What is It and Can it Power Our Society in the Future,” D. Teeters, Invited Speaker, Northeastern Oklahoma State University, Tahlequah, OK, February 11, 2009.

Dale Teeters “Correlation between ion concentrations at the surfaces of PEO films and their casting substrate’s surface free energy,” 11th Annual International Symposium on Polymer Electrolytes, August 2008, Ofir Portugal.

Dale Teeters “PEO-ZnO composite electrolyte system based on oriented ZnO nanorods, “ 11th Annual International Symposium on Polymer Electrolytes, August 2008, Ofir Portugal.

C. Bishop and D. Teeters, “Crystallinity of PEO/Lithium Triflate Complex Confined in Nanoporous Membranes,” 11th Annual International Symposium on Polymer Electrolytes, August 2008, Ofir Portugal.

P. L. Johnson and D. Teeters, “Towards a 3-D Nanobattery System: Individually-wired Nano-electrodes,” Presented at the 14th International Meeting on Lithium Batteries, Tianjin, China, June 2008.

P. Utekar, T. W. Manikas, D. Teeters, “Nanobattery-crossbar system, a promising candidate for future nanoscale data storage,” 208th National Meeting of the Electrochemcial Society, May 18-22, 2008, Phoenix, AZ

S. Maheshwari and D. Teeters, “Template Assisted Nanostructured Battery Electrode Materials,” 208th National Meeting of the Electrochemcial Society, May 18-22, 2008, Phoenix, AZ

T. Manikas and D. Teeters, "Multiple-Valued Logic Memory System Design Using Nanoscale Electrochemical Cells" Presented at the 38th IEEE International Symposium on Multiple-Valued Logic Dallas, Texas, May, 2008

M. Georgy,S. Hulford, R. Sheaff, D. Teeters, “Analysis of osteosarcoma cell growth on alumina, hydroxyapetite, and gelatin nanoscaffolds,” 235th ACS National Meeting, New Orleans, LA, United States, April 6-10, 2008

Dale Teeters “The Molecular Convergence: Bio and Nano Technologies,” Bio Nano Convergence Symposium, Invited Presentation, Tulsa Community CollegeTulsa, OK, September 21, 2007.

Dale Teeters “Nanotechnology: What is it and its Potentially Great Impact on Our Society, Executive Society of Tulsa, Invited Presentation ,Tulsa, OK, September 14, 2007.

Dale Teeters “The Integration of Nanoscale Techniques for an Improved Battery Technology,” ARO Program Review, North Carolina, September 6-7, 2007.

Dale Teeters “Characterization of Mixed Ionic Electronic Conductor Composites Composed of Polymer Electrolyte Confined in Alumina Nanoporous Membranes,” 16th International Conference on Solid State Ionics, Shanghai China, July 1-6, 2007.

Dale Teeters “Polymer electrolytes Confined in nanoporous membranes Exhibiting Mixed Ionic and Electronic Conduction,” Annual State NSF State EPSCoR Conference, Stillwater, OK, May 17, 2007

Number of Presentations: 33.00

Non Peer-Reviewed Conference Proceeding publications (other than abstracts):

Received	Paper

TOTAL:

Number of Non Peer-Reviewed Conference Proceeding publications (other than abstracts):

Peer-Reviewed Conference Proceeding publications (other than abstracts):

Received	Paper

TOTAL:

Number of Peer-Reviewed Conference Proceeding publications (other than abstracts):

(d) Manuscripts

Received		Paper
2012/06/08 1	2	PARAMESWAR HARI, MICHAL BYRCZEK, DALE TEETERS, PRAVIN UTEKAR. INVESTIGATIONS ON THE ELECTRICAL PROPERTIES OF ZnO NANORODS AND COMPOSITES FOR PHOTOVOLTAIC AND ELECTROCHEMICAL APPLICATIONS, International Journal of Nanoscience (11 2011)
2012/06/08 1	5	Matthew R. Smith, Paige L. Johnson, Dale Teeters. Interfacial storage of lithium in the nanostructure of SnO2 nanobaskets for capacities exceeding theoretical values, Solid State Ionics (01 2012)
2012/06/08 1	1	Christina Bishop, Dale Teeters. Crystallinity and order of poly(ethylene oxide)/lithium triflate complex confined in nanoporous membranes, Electrochimica Acta (06 2009)

TOTAL: 3

Number of Manuscripts:

Books

Received	Paper

TOTAL:

Patents Submitted

Nanoscale Three-Dimensional Battery Architecture

Patents Awarded

Awards

Oklahoma Chemist of the Year, 2011-2012

Graduate Students

NAME	PERCENT_SUPPORTED	Discipline
Soumya Yadal	0.50	
Christina Bishop	1.00	
Matthew Smith	0.50	
Daniel Decker	0.50	
Shalini Maheshwari	0.25	
Shawn Nichols	0.13	
FTE Equivalent:	**2.88**	
Total Number:	**6**	

Names of Post Doctorates

NAME	PERCENT_SUPPORTED
FTE Equivalent:	
Total Number:	

Names of Faculty Supported

NAME	PERCENT_SUPPORTED	National Academy Member
Dale Teeters	0.08	
FTE Equivalent:	**0.08**	
Total Number:	**1**	

Names of Under Graduate students supported

NAME	PERCENT_SUPPORTED	Discipline
Christopher Smith	0.04	Chemistry
Daniel Kordonowy	0.15	Chemistry
Daniel Decker	0.02	Chemistry
Lauren Hutter	0.02	Biochemisry
Christina Bishop	0.04	Chemical Engineering
FTE Equivalent:	**0.27**	
Total Number:	**5**	

Student Metrics

This section only applies to graduating undergraduates supported by this agreement in this reporting period

The number of undergraduates funded by this agreement who graduated during this period:	5.00
The number of undergraduates funded by this agreement who graduated during this period with a degree in science, mathematics, engineering, or technology fields:.....	5.00
The number of undergraduates funded by your agreement who graduated during this period and will continue to pursue a graduate or Ph.D. degree in science, mathematics, engineering, or technology fields:.....	4.00
Number of graduating undergraduates who achieved a 3.5 GPA to 4.0 (4.0 max scale):	4.00
Number of graduating undergraduates funded by a DoD funded Center of Excellence grant for Education, Research and Engineering:	0.00
The number of undergraduates funded by your agreement who graduated during this period and intend to work for the Department of Defense	0.00
The number of undergraduates funded by your agreement who graduated during this period and will receive scholarships or fellowships for further studies in science, mathematics, engineering or technology fields:	4.00

Names of Personnel receiving masters degrees

NAME
Soumya Vadala
Shalini Maheshwari
Total Number: **2**

Names of personnel receiving PHDs

NAME
Christina Bishop
Matthew Smith
Total Number: **2**

Names of other research staff

NAME	PERCENT SUPPORTED
Paige Johnson	0.75
FTE Equivalent:	**0.75**
Total Number:	**1**

Sub Contractors (DD882)

Inventions (DD882)

Scientific Progress

Technology Transfer

The Integration of Nanoscale Techniques for an Improved Battery Technology

Army Research Office Grant W911NF-07-1-0398

Final Report

Dale Teeters

Department of Chemistry and Biochemistry

The University of Tulsa

800 South Tucker Drive

Tulsa, OK 74104

The Integration of Nanoscale Techniques for an Improved Battery Technology

Table of Contents

The Integration of Nanoscale Techniques for an Improved Battery Technology

I. Statement of the problem studied

Lithium batteries continue to receive much attention today because they offer a number of significant advantages, both in terms of a high energy density and a large electrochemical window. While today's "gold standard" technology is the lithium ion battery, the lithium polymer electrolyte battery has the potential for even greater capacity. However, there are major problems that must be solved and advances that can be made for both types of battery systems, if these battery systems are to reach even higher performance. These problems are the major reason that while technology associated with electronic devices has advanced at an ever-increasing rate, batteries, the components that makes electronic devices mobile and that allow for novel autonomous operation, have not kept pace with the devices that they power. Battery capacity has not increased substantially since the use of Sony's lithium ion battery technology became wide spread in the early 90s and even then only a relatively small enhancement in technology was observed for battery performance. New advances in battery technology are needed so that the great advances associated with electronic devices such as computer systems, sensors, monitoring systems and other new devices of the future can continue to develop. It is obvious that if battery technology has not substantially progressed for more than a decade, new ideas are needed to improve lithium battery performance. Battery technology is complicated and there is room for improvement in many of the components that make up this power system. Specifically, improvements in the stabilization of the electrode/electrolyte interface (lithium metal batteries), in electrolyte performance and in cell geometry and cathode structure are needed for lithium batteries. Nanoscale science and engineering has the potential to be the mechanism for addressing the concern in all of these areas. The work described here involves the improvement of battery technology by addressing problems in the component parts of batteries by using an integrated nanotechnology approach.

II. Summary of the most important results

Interfacial Storage of Lithium in the Nanostructure of SnO_2 Nanobaskets for Capacities Exceeding Theoretical Values: A nanostructured electrode structure was developed that exhibited stability with respect to cycling and exhibited almost twice the theoretical capacity. An explanation for this added capacity is interfacial storage of lithium at phase boundaries of 2 nm nanoparticles that compose the nanostructure. This fabrication process seems to work for many types of electrode materials and is relatively easy to do. This holds promise for high capacity battery electrodes.

Electrodes with Nanostructured 3-D Architectures and Wiring: A novel 3-D nanoarchitecture consisting of a nanobasket electrode material with nanoscale wiring was

developed. Such a structure helps to overcome problems such as poor transport of electrons from nanostructured electrodes to current collectors, which remains a critical barrier in the use of nanoengineered materials in battery architectures.

Blooming of Wax Surfactants to the Surface of Polymer Electrolytes to Stabilize Passivation at the Lithium Electrode/Polymer Interface: A simple method for placing stabilizing layers at the lithium metal/polymer electrolyte was developed. Molecular layers stabilized the SEI layer formed between lithium metal and the polymer electrolyte. While the molecular protective layer protects against unwanted lithium reactions, the ions appear to be able to move easily through this layer. Stabilizing the lithium metal/electrolyte interface is of critical importance in battery performance.

The fabrication and Characterization of Electrolyte Systems Confined in Nanoporous Membranes for Electrolytes with Enhanced Performance: A novel polymer electrolyte nanostructure consisting of PEO polymer in the form of sleeves or tubes approximately 10nm in thickness in 200 nm pores of AAO membranes was fabricated. The confinement of the electrolyte in this nanostructure increased the ion conduction of the polymer by over 40 orders of magnitude. The possibility of even higher ion conduction is possible, helping to solve one of the problems associated with polymer electrolyte systems.

Integration of Nanostructured and Nanoengineered Technologies into Battery Systems for Maximum Battery Performance: A design for a nanostructured battery that integrates the developments described above was developed

The work summarized above is described in detail below.

III Interfacial Storage of Lithium in the Nanostructure of SnO_2 Nanobaskets for Capacities Exceeding Theoretical Values

III.A. Introduction

Lithium ion batteries are of major technological importance due to their applications as rechargeable power sources for portable electronics. Such batteries exhibit higher capacities and more favorable cycling behavior than typical Ni-Cd and lead-acid battery systems. Unfortunately, lithium metal anodes present safety concerns due to their reactive nature. The most popular anode material is graphite; however, tin oxide is a promising choice for anode material due to its high theoretical discharge capacity, 781 mAh/g, which is more than twice that of graphite, 372 mAh/g [1].

The electrochemical processes that inserts lithium into SnO_2 forming an anode are as follows [2]. At a potential of 1.1 V versus Li/Li^+ SnO_2 is reduced to free Sn, forming Li_2O. This process is irreversible and only occurs during the first charge cycle. At potentials less than approximately 0.7 V, this Sn forms various alloys with lithium, beginning with the simple 1:1 LiSn alloy. As the potential is increased, the maximum of 4.4:1 is reached. During discharge, in

this case removal of lithium, these alloying processes are reversed, producing Li^+ and metallic Sn. These events are summarized below.

Charge processes:

$$SnO_2 + 4Li^+ + 4e^- \rightarrow Sn + 2Li_2O \quad (1)$$
$$Li + Sn + e- \rightarrow LiSn \quad (2)$$
$$LiSn + 3.4Li^+ + 3.4e^- \rightarrow Li_{4.4}Sn \quad (3)$$

Discharge Processes:

$$Li_{4.4}Sn \rightarrow LiSn + 3.4Li^+ + 3.4e^- \quad (4)$$
$$LiSn \rightarrow Li^+ + e^- + Sn \quad (5)$$

It is this 4.4 Li:Sn ratio that gives rise to the maximum theoretical discharge capacity for SnO_2 anodes: 781 mAh/g.

Nanoscale engineering holds great promise for enhancing battery systems and energy storage devices. With SnO_2 nanostructures, the goal is not only to increase surface area for better electrode/electrolyte contact and to shorten path lengths that ions and electrons must travel, but also to prolong electrode lifespan [3-4]. Upon insertion of lithium into the anode, SnO_2 experiences large volume increases, on the order of 300% or more [5,6]. This expansion and the subsequent contraction upon lithium extraction causes compressive and tensile mechanical stress to the electrode, which leads to the formation of cracks that are the primary cause of electrode failure [2, 6]. Many nanostructured SnO_2 materials, such as rods [7], films (8-10), wires [11], and crystals [2), have been reported. If nanotechnology can help alleviate the stress that leads to mechanical degradation caused by lithium intercalation/deintercalation, the cycleability of the electrode would be greatly enhanced so that the high theoretical capacity can utilized in battery systems.

Previous work devised an approach that employs ceramic membranes as templates for self-assembled nanostructures termed nanobaskets. By RF magnetron sputtering, sample material (SnO_2) builds up on the pore walls of a nanoporous membrane, forming columns. Pores of 200 nm have been found to be surrounded by columns that are also 200 nm in diameter. The sputtering process results in nanoparticles that are approximately 2 nm in size, coalescing to form the columns. These columns, composed of the 2 nm nanoparticles, continue to expand outward as they grow and eventually cap over at approximately 600 nm in thickness. The result is an array of nanostructures that each resembles an inverted basket, and these are thus referred to as “nanobaskets” [12,13].

The purpose of this work was to characterize the electrochemical properties and processes for SnO_2 nanobasket anode material for use in lithium ion batteries.

III.B. Experimental

Nanostructured films of SnO_2 were deposited onto nanoporous substrates by RF magnetron sputtering. The substrates used were Whatman anodisc anodized aluminum oxide (AAO) membranes that were 13 mm in diameter and 60 μm in thickness. The membranes had 200 nm pores covering approximately 40% of the surface.

Samples were prepared by RF magnetron sputtering, using a Cressington 208 sputter coater with a Manitou Systems series PB-3 power source. Gold and SnO_2 targets were sputtered at room temperature under approximately 0.01 mbar of argon pressure, with spacing of 7 cm between the target and the sample. The SnO_2 target was 99.7% pure and was a 1/8 inch plate attached to a copper backing plate by indium metal. The effects of sputtering metal oxides, such as SnO_2 onto nanoporous membranes, have been previously reported [12,13]. As described previously, deposits of SnO_2 build up on the pore walls of the membrane, forming columns which grow outward until they cap over. Nanobaskets typically form at around 600 nm in thickness for SnO_2 across 200 nm pores.

First, 150 nm of gold was sputtered onto the membrane. A glass slide was used to cover half the sample while 600 nm of SnO_2 was sputtered onto the unprotected portion. A copper lead was affixed to the exposed gold portion of the sample with silver conductive paste and secured with epoxy. The gold underlayer acts as a current collector between the copper lead and the underside of the SnO_2 layer.

Electrochemical tests were carried out in a glovebox with an argon atmosphere. Samples were analyzed versus lithium ribbon counter and reference electrodes. The electrolyte used was a 20% (w/w) solution of lithium perchlorate dissolved in propylene carbonate. Galvanostatic charge-discharge cycling experiments were conducted, using a MACCOR 2300 at current densities of 1.0 mA cm^{-2} and 0.1 mA cm^{-2} between potentials of 2.0 V and 0.0 V versus lithium. Sample mass was determined so that gravimetric capacities could be calculated. Using a CAHN 29 electrobalance, samples were weighed before and after the sputtering of SnO_2 to determine the amount of active material. SEM micrographs were acquired on a JEOL JSM-840A scanning electron microscope. To reduce sample charging, samples were sputtered with approximately 50-100 nm of gold before being placed in the microscope. Cycled samples were rinsed with isopropanol to remove any adhered electrolyte before sputtering.

III.C. Results and Discussion

<u>Scanning electron microscopy</u>

SnO_2 nanobaskets are shown in Fig. 1. Fig. 2 shows nanobaskets after various stages of cycling. Insertion of lithium into the anode during the charge process causes the material to inflate, expanding in volume. Visual examination of the image correlates well with the 300% expansion reported elsewhere [5,6]. During discharge, lithium is extracted from the anode, causing the nanobaskets to contract, pulling away from each other and forming cracks similar to

those found in a dry creek bed. Further cycling adds to the cracking, leading to smaller islands of material. This mechanical degradation is the leading cause of failure for SnO_2 electrodes.

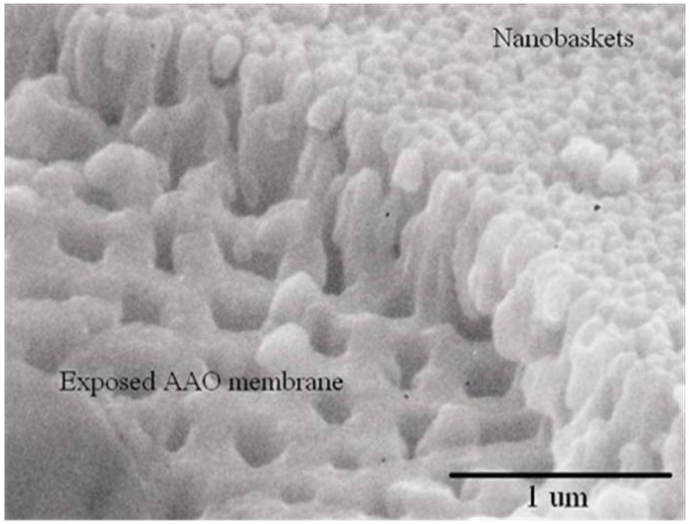

Figure 1. SEM micrograph of SnO_2 nanobaskets. Exposed AAO template material is viewable at left. Nanobaskets are shown on the right.

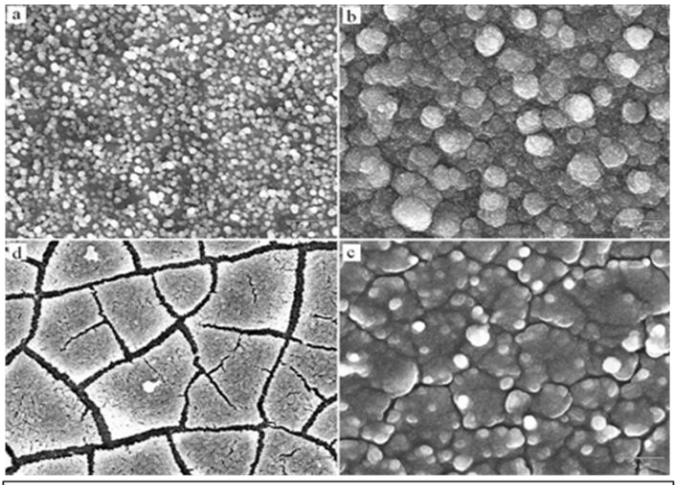

Figure 2. SEM micrographs of SnO_2 nanobaskets sputtered onto templated gold. (a) as prepared, (b) after the first charge cycle, (c) after the first discharge cycle, (d) after 3 charge-discharge cycles. The formation of cracks during cycling causes mechanical degradation that often leads to electrode failure.

Galvanostatic cycling

Galvanostatic charge-discharge curves of SnO_2 sputtered onto gold (Fig. 3) show a variety of plateaus that indicate electrochemical events. Using differential capacity, plotting the

change in capacity with respect to potential (dQ/dV), these plateaus can be better distinguished into peaks representing oxidation and reduction reactions (Fig. 4). During the charge sequence, the reductive peak between 1.0—1.2 V can be attributed to the reduction of SnO_2 and the formation of Li_2O. Further reduction events between 0.6—0.0 V are related to the alloying processes of lithium and tin. The oxidative peaks seen during the discharge cycle reflect the dealloying and extraction of lithium from the anode.

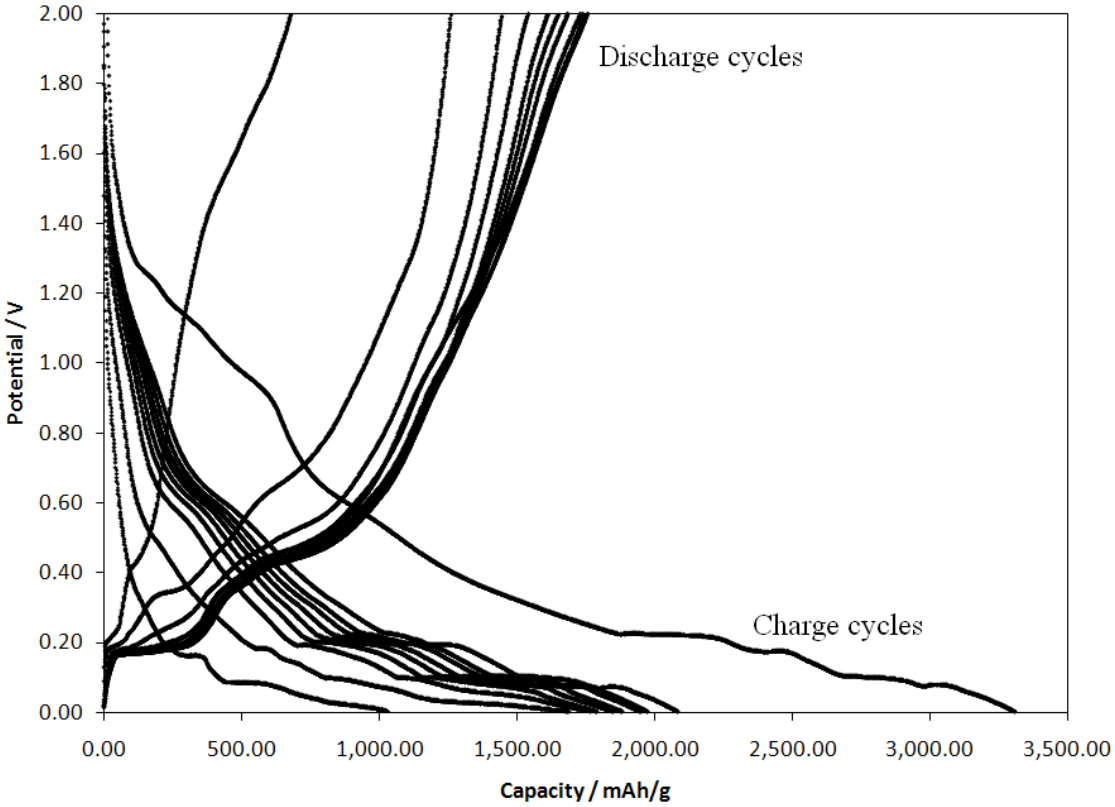

Fig. 3. Galvanostatic cycling curves for the first 10 cycles of SnO_2 nanobaskets sputtered onto gold, showing capacities above the theoretical limit for SnO_2 alloying with lithium.

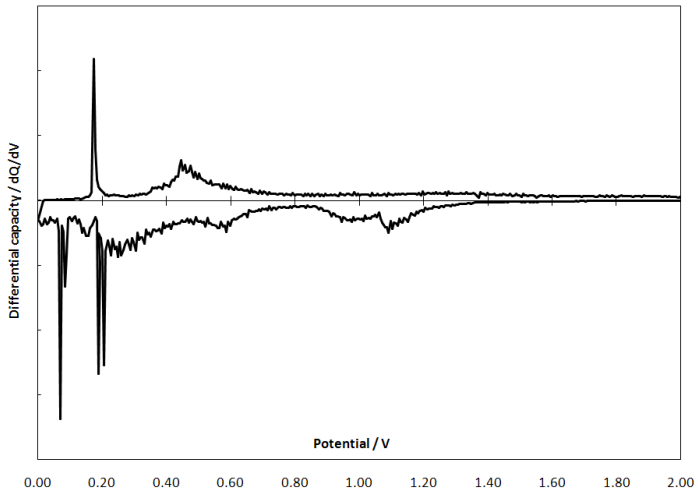

Fig. 4. Differential capacity plot of SnO_2 nanobaskets sputtered onto gold. The sharp reduction peaks at 0.2 V and 0.08 V and the oxidation peak at 0.18 V do not normally appear for bulk SnO_2 anodes.

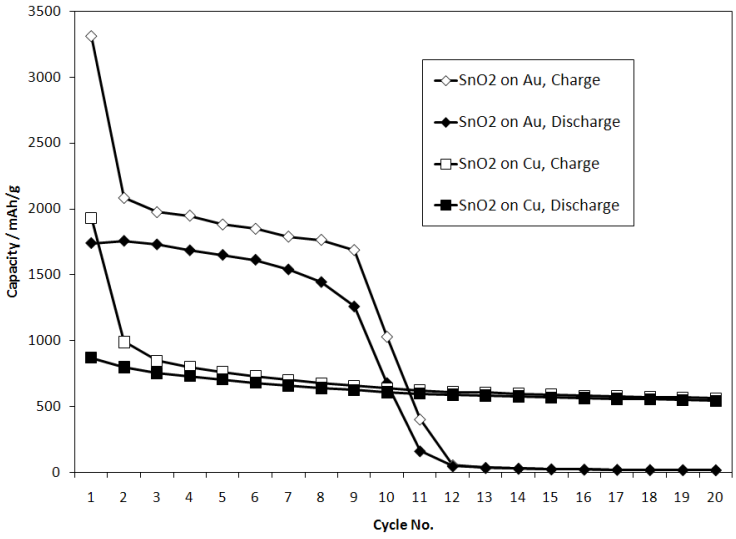

Fig. 5. Cycle capacities for SnO_2 nanobaskets sputtered onto gold compared to those sputtered onto copper, showing unusually high capacities for the gold-layered SnO_2 nanobaskets and the favorable cycling behavior of the copper-layered SnO_2 nanobaskets. Gravimetric capacities are listed per gram of SnO_2.

The final reduction peaks during the charge cycle at 0.2 and 0.08 V, and also the first oxidation peak of discharge at 0.18 V, are of special interest because they do not appear on cyclic voltamograms or charge-discharge curves for bulk SnO_2 anodes [2, 10]. This may be evidence that there are other processes occurring in the nanobasket electrodes.

Discharge capacities are shown in Fig. 5. SnO_2 nanobaskets sputtered onto gold show exceptionally high discharge capacities, over 1730 mAh/g. This is more than twice the theoretical capacity based on alloying, 781 mAh/g. Possible explanations of this phenomenon will be discussed below. The sample shown is capable of maintaining this capacity for approximately 10 cycles before decreasing to near zero. In recent work, we have had samples maintain capacities above theoretical for as many as 60 cycles at a 1C rates.

Investigation of anomalous capacity

To investigate the source of this added capacity, we looked to other components of the sample preparation: the anodized alumina membrane and the gold underlayer. The following samples were prepared and cycled: bare AAO membranes, AAO membranes sputtered with a thin layer of gold, and AAO membranes sputtered with a thin layer of copper. Cycle capacities of these components are show in Fig. 6.

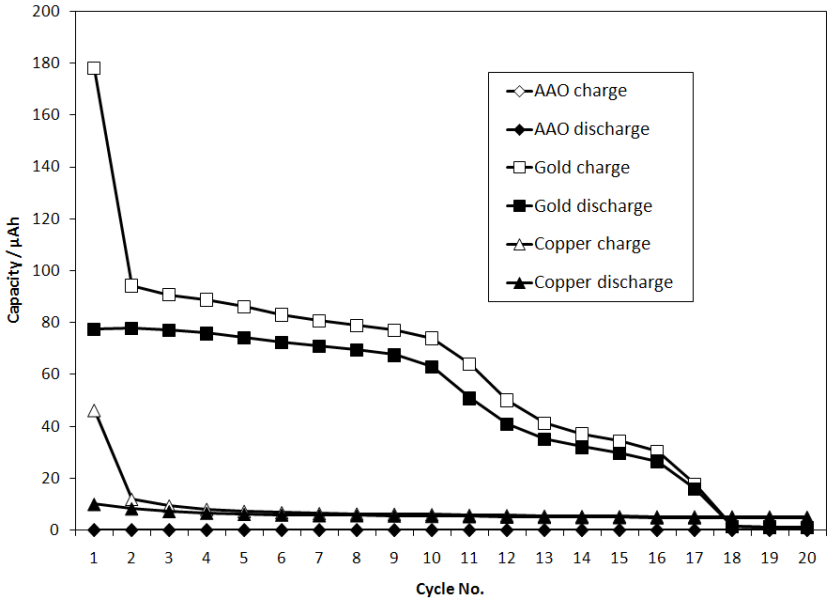

Fig. 6. Cycle capacities for the bare AAO membrane, gold sputtered AAO membrane, and copper sputtered AAO membrane. The bare AAO membrane and copper layer show negligible discharge capacity, confirming that they do not form alloys with lithium or contribute significantly to the discharge capacity of SnO_2 nanobaskets.

Galvanostatic cycling of the bare alumina membranes reveals a very small charge capacity and a negligible discharge capacity. This indicates a small irreversible reaction, which we theorize is due to lithium reacting with surface hydroxyl groups on the alumina, forming Li_2O. Regardless, it is clear that the AAO membranes do not provide any significant contribution to the discharge capacity. Analysis of the gold layer reveals that the additional peaks seen in the cycling curves and differential capacity plots are due to the gold layer forming alloys with lithium, as seen by comparing Fig.s 4 and 7. The gold layer, approximately 150 nm in thickness,

sputtered onto the AAO membranes, was capable of a reversible discharge capacity of 180 mAh/g compared to the theoretical value of 261 mAh/g based on the $Au_{60}Li_{40}$ alloy [14].

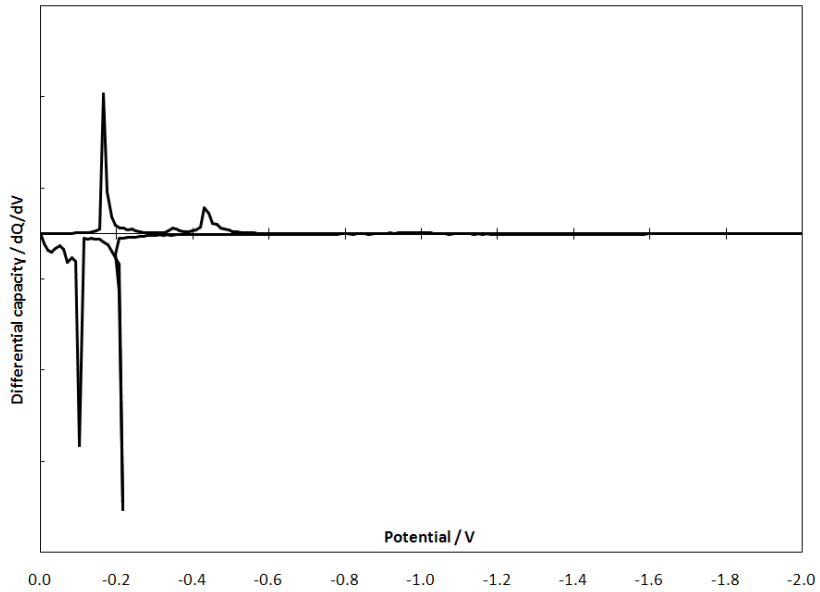

Fig. 7. Differential capacity plot of the gold sputtered AAO membrane. Major peaks show reduction at 0.2 V and 0.1 V and oxidation at 0.17 V, which match the anomalous peaks found in Fig. 4.

Because it is clear that the gold layer does form alloys with lithium, using copper allows us to isolate the capacity of the SnO_2 nanobasket layer alone. As shown in Fig. 8, SnO_2 sputtered onto copper shows a reversible capacity of 1500 mAh/g, over the theoretical capacity of 781 mAh/g. The anode also shows good cycling behavior, keeping a capacity over the theoretical value for over 60 cycles. The differential capacity plot, shown in Fig. 9, also more closely resembles that for bulk SnO_2 anodes [2, 10]. That SnO_2 sputtered onto copper shows slightly lower capacity but better cyclability than SnO_2 sputtered onto gold suggests that the expansion and contraction of the gold underlayer upon insertion and extraction of lithium may be a leading contributor to mechanical degradation and electrode failure.

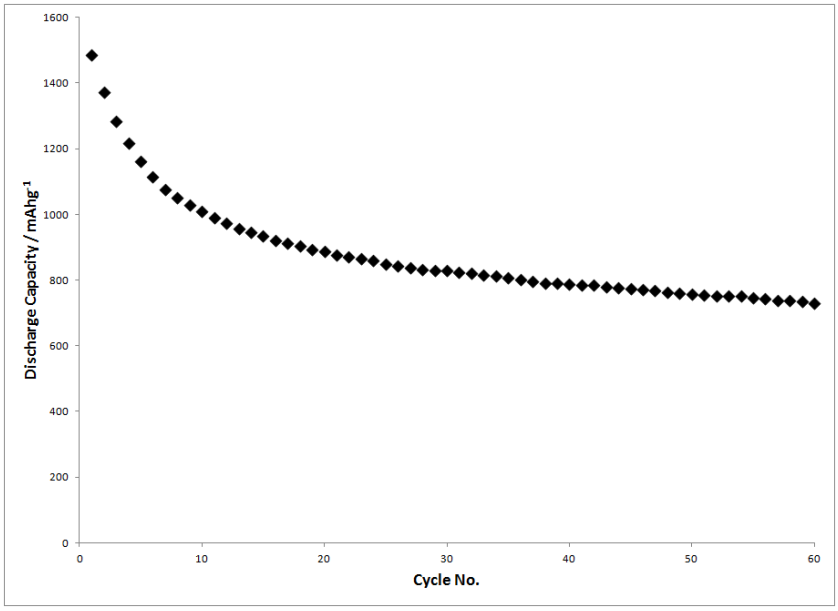

Fig 8. Discharge capacities for the first 60 cycles of SnO_2 sputtered over Cu-coated AAO.

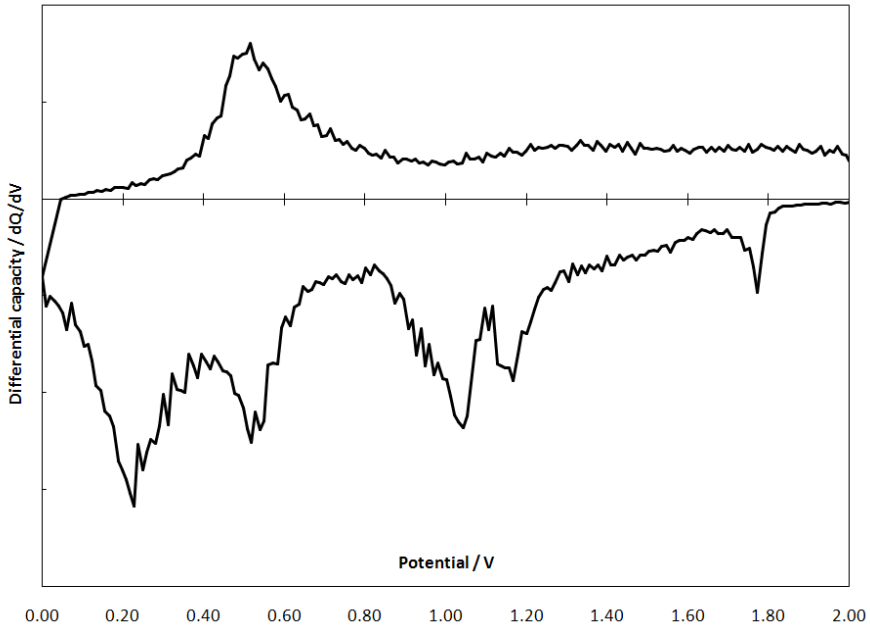

Fig. 9. Differential capacity plot of SnO_2 nanobaskets sputtered onto copper. The reductive peak at 1.75 V is due to the copper layer, but accounts for only 2% of the charge capacity and only appears during the first cycle.

Interfacial Lithium Storage

Even with the removal of the anomalous contribution from the gold under layer, the capacity of the SnO2 is still higher than the theoretical capacity. One possible explanation of

this could be that the nanostructuring of the electrode allows the LiO_2 formation to become a reversible step. If this were reversible, extra capacity would be found, since lithium could be stored, forming LiO_2, and then reversibly removed. However, differential capacitance studies done by our group have shown that the LiO_2 once formed does remain irreversible [15]. Another possible explanation for this is interfacial charging. Maier et al [16-20] describe a phenomenon upon which lithium ions collect at phase boundaries, resulting in both battery and capacitor like properties. Materials with high surface/volume ratios, such as nanostructured materials, would be expected to show enhanced lithium storage in this manner [17]. Because the nanobaskets have a substructure of nanoparticles only 2 nm in size, they possess an extremely high surface/volume ratio, and thus a great potential for interfacial storage of lithium. To investigate this phenomenon, samples of SnO_2 sputtered over Cu-coated AAO membranes were prepared and then annealed at 500 °C for 5 hours. Annealing the samples at 500 °C has been shown to soften the SnO_2 layer, causing the nanoparticles to coalesce into a more bulk form. The smaller nanostructure, nanoparticles on the order of 2-4 nm in diameter, is eliminated while the larger nanostructure would was not affected. Thus, the tests will reflect samples that are identical in their chemical composition, only differing in the smallest level of nanostructuring.

Galvanostatic cycling (Fig 10) shows a drastic decrease in capacity for the annealed nanobaskets, from initial values of 1480 $mAhg^{-1}$ for the -prepared nanobaskets to 560 $mAhg^{-1}$ for the annealed set. This is a change in capacity which can only be due to a quenched potential for nanoparticle interfacial charging resulting from the coalesced structure after annealing. Such an interpretation of the nanoparticle substructure correlates well with Raman spectroscopy studies. Raman spectra obtained from the nanobasket structure described here have confirmed that it is the substructure of the electrode, the nanoparticles on the order of 2nm, which coalesce back into the bulk form upon annealing [13]. It must be assumed that these nanoparticles are responsible for a very large interfacial surface area of the electrode system, and must account for the excessive capacity of the SnO_2 nanobasket electrode material in the form of interfacial storage of lithium.

The annealed samples warrant further discussion. Even though the capacity has been reduced below the theoretical capacity after heating, the capacity remains remarkably constant, around 340 $mAhg^{-1}$. This is a very good capacity when compared to that of graphite, which makes this structure interesting. Our studies show that after annealing, the pores shown in Fig. 1 still remain even though the subnanostructure comprised of the 2 nm particles has coalesced [15]. This nanostructure seems to be sufficient to allow the SnO_2 to expand and contract without destruction of the electrode, a stability that has been seen for other nanostructured electrodes [21]. Indeed, the fact that the structure investigated here can endure for more than 60 cycles shows the benefits of nanostructuring for resistance to electrode deterioration due to cycling. This structure in itself deserves further study.

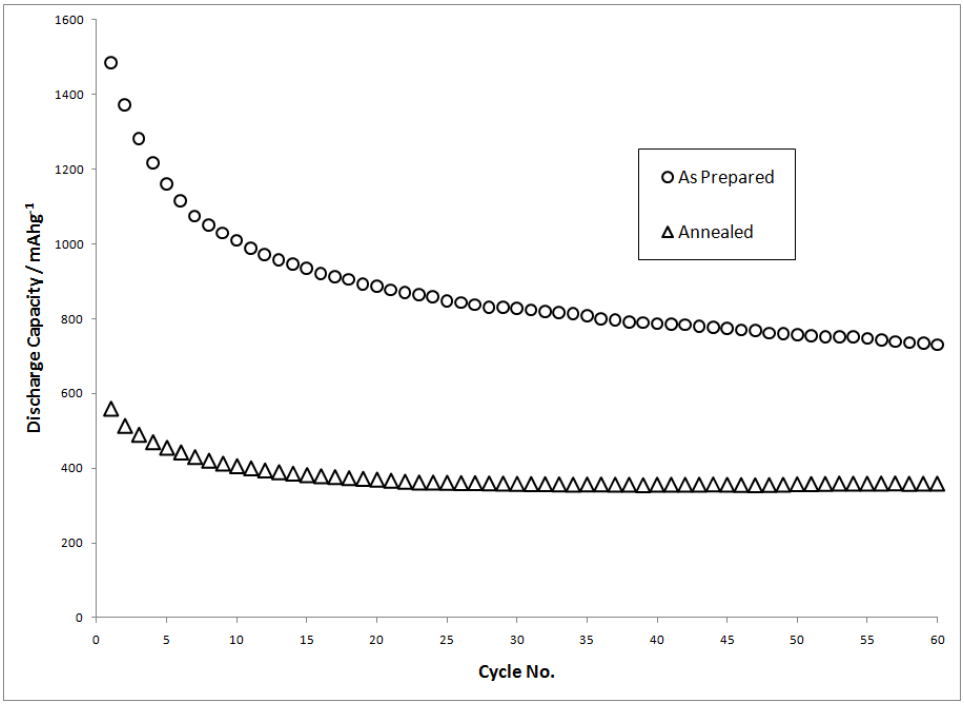

Fig 10. Discharge capacities for SnO_2 nanobaskets as-prepared and after annealing at 500 °C.

III.D. Conclusions

A study was made of SnO_2 nanobaskets sputtered onto two different metal current collector layers. SnO_2 nanobasket electrodes sputtered onto gold showed unusually high capacities, almost twice the theoretical limit for SnO_2 based on alloying with lithium. An explanation for this added capacity is interfacial storage of lithium at phase boundaries. SnO_2 sputtered onto copper shows favorable cycling behavior, maintaining capacities almost twice the theoretical value after more than 60 cycles.

IV. Electrodes with Nanostructured 3-D Architectures and Wiring

IV.A. Introduction

The assembly of individual nanostructured components into a three-dimensional (3D) battery system has been proposed as the means to promote ion diffusion in electrode materials by substantially increasing the effective electrode surface area [22, 224] to improve energy per unit area characteristics and promote a high rate charge/discharge capacity. Such features should enhance general battery performance. Recent work on 3D architectures for improved performance includes rods or "posts" connected to a substrate [23, 24], graphite meshes [23, 25] and films of cathode, electrolyte and anode materials lining microchannels in an inert substrate [26, 27]. A comprehensive review of these architectures, both studied and proposed, can by found in the work by Long, Dunn, Rolison and White [23].

One of the difficulties in creating effective 3D architectures lies in the conflicting geometric goals for high capacity and low resistance [23]. When utilizing micro-rods or micro-

plates of electrode material extending from a substrate into the electrolyte, for example, capacity increases as the length, L, of the rods or plates is increased but electronic resistance also increases with L, limiting overall system performance. In many 3D architectures, therefore, a tradeoff between efficient ion diffusion and electron conduction must be made. The structure described in this work addresses these concerns by combining a nanostructure that presents a high surface area for ion diffusion with nanoscale wiring to reduce ohmic resistance.

Previous research has documented the construction of nanostructured oxide films by RF-magnetron sputtering onto a nanoporous anodized aluminum oxide (AAO) substrate [13]. During sputtering, thickened columnar growths form around the pores of the substrate, essentially extending the pores with the oxide material. The diameter of these columns is dependent on the diameter of the substrate pores and they grow thicker as they extend upward, eventually growing together to form caps over the empty pore spaces (Fig. 11). We have termed these structures "nanobaskets." Raman spectroscopy has revealed that the nanobaskets have a substructure of coalesced nanoparticles whose size is on the scale of 2 nm [13]. It has been demonstrated that electrodes composed of such small nanoparticles show better cycleability [28, 29] and a greater initial specific battery capacity [30]. The purpose of this work is to enable effective electrical contact with the nanobaskets by individually wiring them to maximize electron flow.

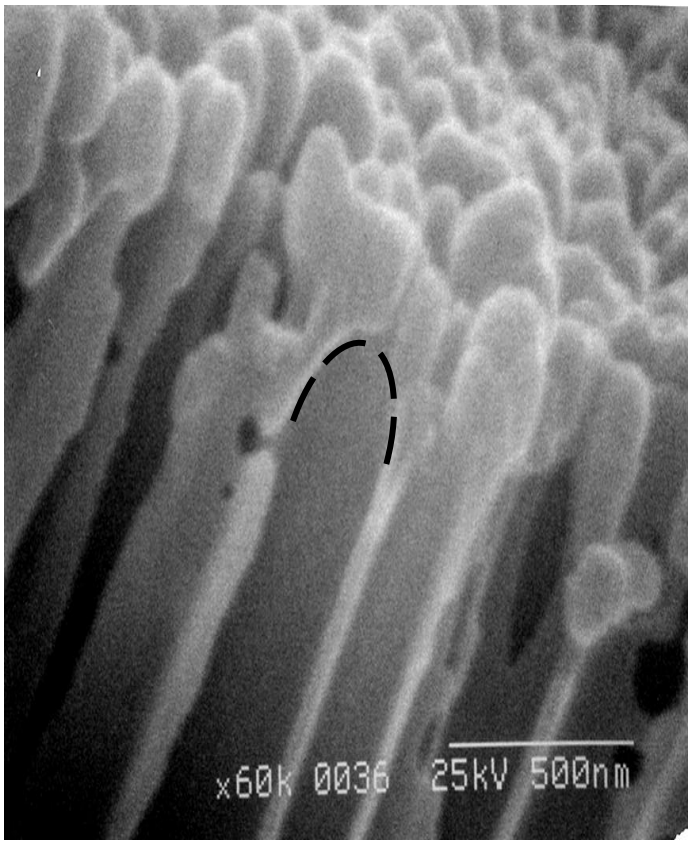

Fig. 11. SEM image of a cross section showing empty SnO_2 nanobasket atop alumina pore. The dotted line delineates the interior surface of the nanobasket.

IV.B. Experimental

Electrodes of SnO_2 and $LiCoO_2$, as well as layered systems of Au plus those same oxides were sputter coated onto Whatman Anodisc membranes with 200 nm pore sizes, using a Cressington 208 sputter coater with a Manitou power source. The complete procedure for this process can be found elsewhere [13]. Electrochemical deposition, utilizing a standard, three-probe electrochemical cell as delineated in procedures published by Wu et al, Gao et al, and others [31, 32], was used to grow copper nanowires from the nanobasket electrode layers and

into the 200 nm pores, ultimately extending through the entire 60 micron thickness of the AAO membrane. A Parstat 2273 potentiostat was used to apply a DC voltage of -0.15 V for 6 hours, generating nanowires from an aqueous solution 0.5 M in $CuSO_4$ and 0.1 M in boric acid. SEM images were taken with a JEOL 840A and ac impedance data from 0.1 to 106 Hz was collected, using a Solartron 1260 gain/phase analyzer equipped with a 1296 interface.

AAO membranes with 200 nm pore sizes, forming copper nanowires of the same diameter, were selected for this experiment, since copper nanowires smaller than 100 nm diameter have a higher resistance, due to being close to the mean free path of electron diffusion in copper metal [33, 34].

The DC method of growing wires through AAO nanoporous membranes is very dependent on cleanliness of surfaces and complete wetting of the channels of the AAO membrane. The complete filling of all the wires in a given AAO membrane has been found to be difficult within the context of this work as well as elsewhere [35]. To maximize pore filling, the membranes were ultrasonically agitated in deionized water for 15 minutes, then placed in the aqueous solution of the electrochemical cell for another 15 minutes prior to the application of voltage for electrodeposition.

IV.C. Results and Discussion

In order to practically enable electrical contact with the nanobasket structure, the nanowires need to grow from the baskets and completely through the AAO membrane to the opposite side, as shown schematically in Fig. 12. It has been reported that the growth of metal nanowires through AAO membranes is facilitated by the presence of a thin gold layer [31] so a

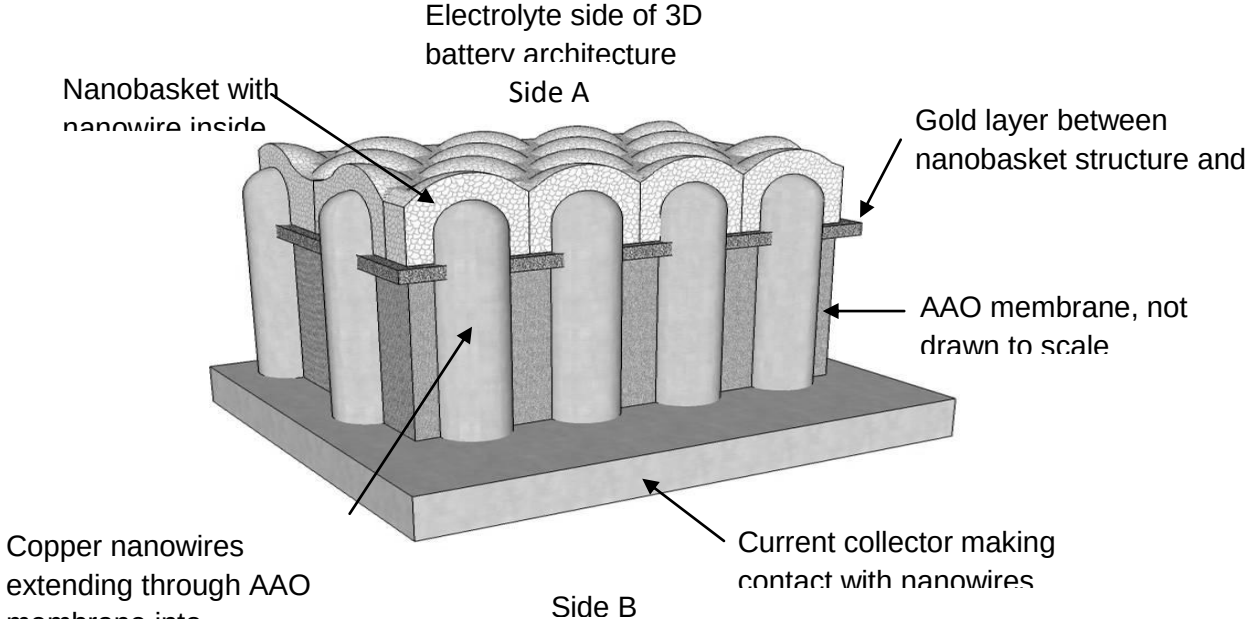

Fig. 12. Schematic of 3D nanobattery architecture.

100 nm layer of gold was sputtered on the AAO membrane prior to deposition of the nanobaskets. Previous work [13] has shown that it is possible to grow the nanobasket structure on top of such a metallic layer. The gold film deposited on the AAO membrane served as the nucleation site for growth of the copper nanowires from the nanobaskets, through the membrane's 200 nm pores and out the untreated side of the membrane. Nanobaskets of both the anodic material SnO_2 and the cathodic material $LiCoO_2$ have been successfully nanowired, using this electrochemical deposition technique.

Fig. 13 shows a broken cross section of an AAO membrane with electrodeposited copper nanowires, some of which are bent and pulled out of their pores. The copper nanowires were observed extending from the nanobasket layer and through the entire length of the membrane, a configuration which allows an external current collector to make contact with the nanowires and in turn with the nanobasket electrode (see Fig. 12). Fig. 14 shows the nanobasket-nanowire contact at higher resolution, with insertion of the nanowire into the nanobasket clearly visible. Contact of the nanowires with the nanobaskets was confirmed by ac impedance spectroscopy. The wired membrane was placed between two stainless steel electrode plates so that contact was made with the nanobasket electrode layer on one side (Side A in Figs. 12 and 13) and the 200 nm diameter wires protruding from the nanobasket structure on the other (side B in Figs.. 12 and 13) If the nanowires are in fact making electrical contact with the nanobasket structure, an ac impedance spectrum indicative of the metallic oxide should be observed. The features exhibited in Fig. 15 are indicative of a SnO_2 layer on the AAO substrate as seen in previous work [13]: a prominent semicircle and low frequency and a faint inflection at high frequency (Fig.15 inset). These high and low frequency features have been attributed to the bulk and grain boundary conduction respectively [36] and are consistent with that seen in previous work in which the SnO_2 nanobaskets were contacted through a continuous current collector, not through nanowires [13].

Fig. 13. SEM image of a cross section of an AAO membrane containing copper nanowires grown from a $LiCoO_2$ nanobasket layer.

The existence of the very large grain boundary feature, completely overshadowing the bulk contribution, has been attributed to the presence of

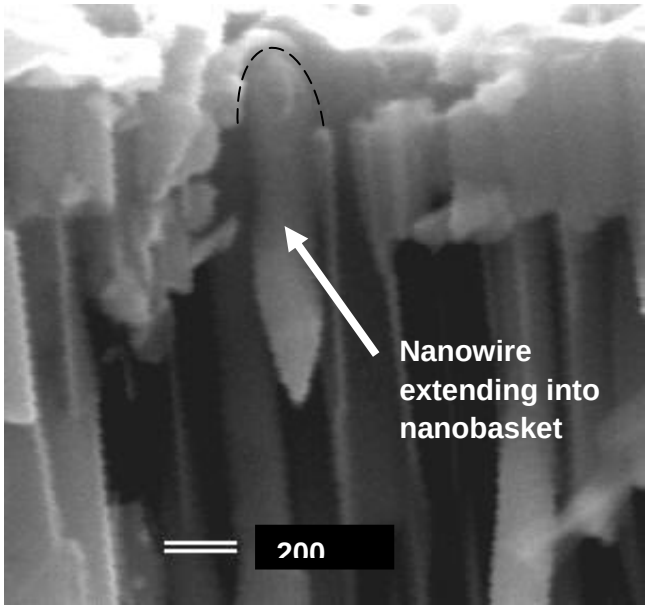

Fig. 14. SEM image of a cross section of SnO_2 nanobasketfilled with a copper nanowire. The dotted line delineates the interior surface of the nanobasket.

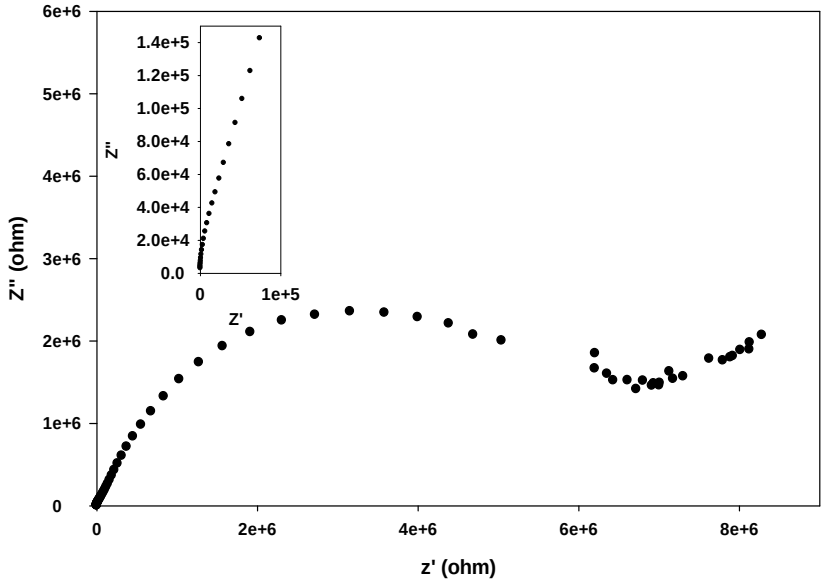

Fig. 15. Nyquist plot of the nanobasket layer. The inset shows the high frequency region in more detail.

the 2 nm nanoparticles comprising the nanobasket structure and creating an extremely large interfacial area [13].

Previously observed conductivity values for the SnO_2 nanobasket structures, acquired through a continuous current collector layer, were 1.5 x 10^{-8} S cm^{-1} [13]. These are in agreement with subsequently published data on the conductivity of SnO_2 nanostructures which showed conductivities of 6.0 x 10^{-8} S cm^{-1} for SnO_2 nanotubes of 100-300 nm diameter and 1.2 x 10^{-8} S cm^{-1} for SnO_2 nanopowders of 100 nm and less [37]. The calculated specific conductivity for the nanobasketed SnO_2 film in this work, acquired through the nanowires, was 1.8 x 10^{-11} S cm 1. SEM images showed that nearly all nanowires were in excellent contact with the nanobasket structures, but that not all were long enough to exit the untreated side of the membrane (side B Fig.12). More work remains to be done in getting all wires to grow outside the AAO membrane for electrical contact; however, the ability to wire individual nanobaskets in the electrode system, and their effective use to make electrical contact, has been demonstrated.

The individual wiring of nanobaskets has distinct benefits. Long et. al. [23] have used the dimensionless number, U, described in the equation below, to analyze electrode performance.

$$U = \left(\frac{w^2}{L^2}\right)\left(\frac{\mu}{\sigma}\right)\left(\frac{1}{C}\right) \qquad (6)$$

Here w is either the diameter of rods or the thickness of plates in a 3D microelectrode architecture, L is the length of the rods or height of the plates, μ is the ionic mobility of the cations in the electrolyte, σ is the electronic conductivity of the electrode material and C is the volumetric energy capacity. U serves to describe the uniformity with which the electrode is utilized. The smaller U becomes the more uniform is the current distribution along the electrode. Lowering the value of μ, would mean hindered ion conduction, so large L values with high σ values are desirable for minimizing U and maximizing electrode performance.

The structure discussed in this work, schematically shown in Fig. 11 and in SEM images (Figs. 12 and 13), maximizes these parameters for improved electrode performance. The interior surfaces of the electrode material's 200 nm diameter nanobaskets are in intimate contact with the metal nanowires, providing a high effective σ value. Additionally, the L term in Eq. 6 is maximized by the exterior surface of the nanobaskets, which would be the surface in contact with the electrolyte in a 3D battery configuration. This exterior surface, which can be thought of as a topography of upside-down nanobasket 'caps', presents a high surface area for electrolyte contact. Fig. 16 is

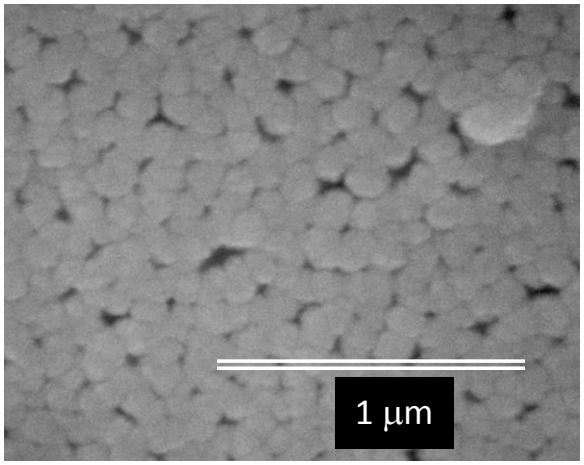

Fig. 16. SEM image of the top of the nanobasket structure. Fissures can be seen extending down between the columns that make the nanobaskets.

an SEM image of this surface, demonstrating its highly roughened nature, with fissures between the individual nanobaskets caps readily seen. Both the curved nanobasket caps and the fissures between them make a high surface area available for electrolyte contact, which will enhance ion diffusion into the electrode material and complement the augmented electronic conduction resulting from the nanowires inside the nanobaskets.

IV.D. Conclusions

Though a wide range of research efforts are directed at nanostructuring the separate components of lithium battery systems, only a few attempt to assemble a battery that is nanostructured in all its dimensions exist. Poor transport of electrons from nanostructured electrodes to current collectors remains a critical barrier to the use of nanoengineered materials in battery architectures. We have successfully assembled and made electrical contact with a novel 3-D nanoarchitecture consisting of a nanobasket electrode material with nanoscale wiring.

V. Blooming of Wax Surfactants to the Surface of Polymer Electrolytes to Stabilize Passivation at the Lithium Electrode/Polymer Interface

V.A. Introduction

Improvements for the lithium metal-polymer battery, the battery touted as having the most potential for future enhanced performance battery systems [38], are necessary for this battery to reach its full technological importance. For instance, improvement and an understanding of the stabilization of the metal electrode/polymer electrolyte interface are needed for maximized performance of lithium polymer batteries. The formation of an electrolyte inter-phase layer or SEI layer is well known in lithium ion batteries with liquid electrolytes [39-46], but it also can manifest itself at the interface between lithium metal and polymer electrolytes. With time, the interfacial impedance can grow until it is significantly larger than that of the polymer electrolyte, which is usually thought of as the main source of resistance in polymer electrolyte batteries [47,48]. The unstable SEI layer becomes more and more impervious to ion conduction and results in poor battery performance.

There have been many studies of processes involving lithium or lithium alloy anodes in contact with electrolytes consisting of lithium salts complexed with poly(ethylene oxide) polymers [49-55] or plasticized PEO polymers [56]. These studies clearly show the presence of a resistive layer. It was initially thought that this layer may be due to trace quantities of water, but work done by Fauteux [57] on ultra dry films proved this to not be the case. A.C. impedance data collected by Bruce's group [48] suggested that surface layers develop on both electrode interfaces, as indicated by the increasing interfacial impedances. The authors were able to eliminate the possibility of an impurity contribution to this interfacial impedance, but the nature of the surface layer was not determined. Hiratani et al. [58] investigated the interface between lithium and a polymer solid electrolyte consisting of a thin film (150 nm) of PEO complexed with 9 mole % LiCF3SO3. These studies also utilized complex impedance spectroscopy and indicated an increase in the interfacial resistance, which was attributed to a charge transfer process. Vincent's work shed light on the chemical processes involved [59]. He proposed a

chemical mechanism for a PEO polymer electrolyte containing LiSO3CF3 reacting with a lithium metal electrode. The reaction of lithium triflate with lithium metal as shown in the following reaction:

$$LiSO_3CF_3 + Li\ (s) \rightarrow 2Li+ + SO_3^{2-} + CF_3\cdot \quad (7)$$

Vincent proposed that the CF_3 radical could then extract a hydrogen atom from the PEO polymer chain forming HCF_3 and perhaps result in the breaking of the polymer chain. Surface IR spectroscopy has shown this to be the case followed by the formation of organo lithium compounds. A proposed mechanism is [49]

$$CF_3\cdot + \text{-}CH_2\text{-}CH_2\text{-}O\text{-} \rightarrow HCF_3 + \text{-}CH{=}CH\text{-}O\text{-} + H\cdot \quad (8)$$

$$Li(s) + \text{-}CH_2\text{-}OCH_2\text{-} + H\cdot \rightarrow \text{-}CH_2\text{-}O\text{-}Li + CH_3\text{-}R \quad (9)$$

PEO/lithium triflate polymers that have been in contact for only 15 minutes with a lithium electrode already show chain scission presumably by this mechanism, and after 21 hours contact with the lithium electrode, Li-O-R and Li-O-R-O-Li compounds begin forming [49].

There have been numerous attempts to address the problem of an unstable lithium/electrolyte SEI layer, especially in liquid electrolyte systems. One way to approach this unstable passivation layer problem in liquids is to modify the interface with emphasis being placed on the lithium metal surface. Techniques, such as polymer coatings [60-63], various electrolyte additives such as CO_2, N_2O, HF and SO_2 [23, 62, 64, 65] or organic compounds [63,66,67] have been evaluated. Recently, reactive silane derivatives have been used with lithium to stabilize the SEI [68,69]. Visco and Chu have protected the lithium surface by using plasma assisted deposition techniques to place a very thin glassy coating on the lithium metal surface [70, 71].

Polymer electrolyte systems with similar methods of SEI stabilization to that of liquid electrolytes have been the objects of investigation. For instance, modifications of the electrolyte composition have been used to stabilize the lithium metal/polymer electrolyte interface. Scrosati's group has shown that the addition of inert, ceramic fillers such as Al_2O_3 and TiO_2 to the electrolyte will stabilize the interface [72,73] while Itoh reported that particles of LiAlO2 added to PEO electrolyte improved electrochemical compatibility with a lithium metal electrode [74]. Hyperbranched polymers and dendrimers can also have beneficial effect on stabilization. A hyperbranched polyester improved interfacial performance when compared with PEO alone [75]. Watanabe reported that methyl ether chain ends in crosslinked comb PEO electrolytes reduced charge transfer resistance at the lithium electrode interface [76]. However, no explanation for these observations has been given. Self-assembled molecular, SAM, layers were adsorbed on a PEO electrolyte where the self-assembled hydrocarbon chains on the surface form a layer, that when in contact with lithium, is resistant to reactions that destabilize the SEI [49-51, 77, 78].

It is this self-assembled approach that is the subject of this study. In previous studies, polymer electrolytes with SAM protective layers were made by using an adsorption from solution process of molecules where half the molecule, which is PEO-like, wants to adsorb into the solid polymer while the other half of the molecule is a hydrocarbon chain that self-assembles at the polymer electrolyte surface [49-51, 77 78]. The hydrocarbon chains were found to align perpendicular to the surface assembling into a parallel chain structure with considerable crystallinity [49]. While these protected films were shown to be stable with respect to lithium metal, both under open circuit [49-51, 77] and electrochemical cycling [78], the fabrication of these lithium-stable films is complicated because of the solution adsorption process. A simpler method is a single step film casting technique where the electrolyte films are prepared by casting a solution composed of the PEO polymer electrolyte, inorganic salt and the molecule that forms the self-assembled layer. The molecule forming the SAM could be expected to "bloom" to the surface during removal of the solvent as the film is formed because of the difference in free energies between the forming bulk film and its surface. This difference would "pull" the SAM-forming molecule to the polymer/gas interface where it would self-assemble, forming the protective layer. Not only is this a simpler method of fabrication of lithium-stable polymer electrolyte film, but it could lead to understanding of how other polymer electrolytes with additives such hyperbranched polymers and dendrimers [75,76] and polyether surfactants [61] stabilize the SEI layer. A novel way of observing the stabilizing molecules at the surface using AFM phase imaging is also discussed.

V.B. Experimental

Poly(ethylene oxide) (PEO), from Sigma-Aldrich with a molecular weight of 1,000,000, was mixed with Lithium trifluoromethanesulfonate 96% (lithium triflate), from Aldrich Chemical, in such proportions that the ether oxygen/lithium ion ratio was 15/1. The mixing took place in ACS certified acetonitrile, which was obtained from Fisher Scientific. The ratio of milliliters of solvent to grams of PEO was 100/1. Standard films, containing none of the wax surfactant, were made by simply mixing all the above with a magnetic stir bar and stirring plate until the solids are completely dissolved in the solvent. The solution is then poured into a Teflon substrate and placed in an evaporation chamber with nitrogen gas flowing through constantly until evaporation of the solvent results in a film of the PEO electrolyte. When the film is dry, it is placed in an argon atmosphere glove box for at least 24 hours before testing. The molecular self-assembled layer was formed by a compound having the chemical formula $H\text{-}(\text{-}CH_2\text{-})_{32}\text{-}(\text{-}CH_2\text{-}CH_2\text{-}O\text{-})_{10}\text{-}H$. This material is a wax-like solid and has surfactant properties because of its nature to move to interfaces. Because of it being a waxy solid, it will be referred to as the "wax" throughout the rest of this paper. The wax was procured from the Baker Petrolite Polymers Division of Baker Hughes. To make a film containing the wax, the procedure for the standard film is followed except for the addition of varying amounts of a second acetonitrile solution containing the monolayer forming molecule. This saturated solvent containing the wax is made by simply mixing the wax and the solvent together to form a suspension. After allowing the wax/acetonitrile solution to sit for a day, the suspended wax falls to the bottom of the flask and the turbid saturated solution that is left can be collected by using a pipette, being careful not to disturb the solid sitting on the bottom of the flask. By the addition of this standard wax solvent mixture, films can be made with varying concentrations of the wax material in the polymer. The

films were examined, using a Solatron SI 1260 impedance/gain-phase analyzer and solatron 1296 Dielectric Interface, varying the frequency from 1.000 MHz to 100 mHz, Veeco atomic force microscope with a Nanoscope V controller, as well as Avatar multi-bounce HATR 360 FT-IR. Using these instruments, film impedance, AFM topography and phase images and IR surface composition measurements were made. Film impedance for various lithium/PEO/lithium cells, were measured for a time period of up to two days. Measurements were made between stainless steel blocking electrodes. A screw was used to place constant pressure of 60 KPa, as read by torque sensor, on the two blocking electrodes, and was checked daily to insure a constant force between the lithium and the electrolyte.

V.C. Results and Discussion

Films consisting of the pure PEO polymer electrolyte and polymer electrolyte having wax concentrations of 2, 4, 6 and 8% by mass were studied. These concentrations were chosen so that there would be enough wax to bloom to surface, but a small enough amount so that there would be little change in the physical properties of the film.

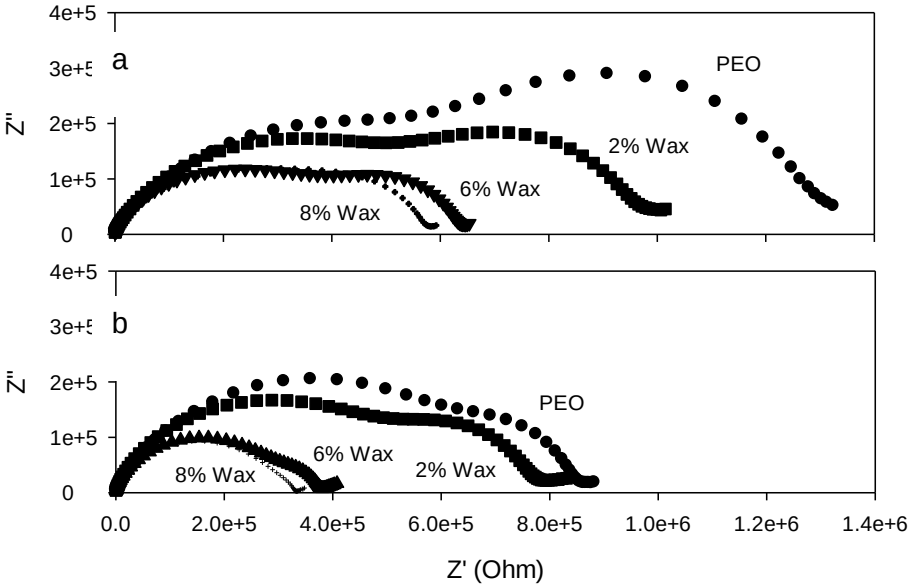

Fig. 17. AC impedance data for pure PEO electrolyte and electrolyte with varying amounts of wax in a Li/polymer electrolyte/Li symmetric cell. Fig. a shows data for polymer electrolyte that has been exposed to lithium for 2 days. Fig. b is data after less than 10 minutes exposure to lithium, i.e. initial conditions.

Fig. 17 shows ac impedance data for representative symmetric Li/polymer electrolyte/Li cells under open circuit conditions. Only data for the pure PEO and PEO with 2, 6 and 8% wax are shown for sake of clarity. Fig. 17a is data for polymer electrolyte films that has been in contact with lithium metal for two days while Fig. 17b shows the films approximately 10 minutes after assembly, i.e. initial conditions. The high frequency semicircular features are attributed to the bulk polymer electrolyte as has been assigned in ac impedance experiments

conducted on similar systems [49, 50, 77]. The second, lower frequency feature is attributed to the SEI layer [49, 50, 77]. Even the initial data collected in under 10 minutes of contact with lithium (Fig. 17b) show the presences of significant interfacial resistance due to the SEI. However, at the higher concentrations of wax, the resistance due to the SEI is much less. It is especially small for the polymer electrolyte with the most wax, 8%. It is not surprising the unprotected films and the films with small amounts of wax would have higher resistance at the interface since previous work has shown that PEO/lithium triflate polymers that have been in contact for only 15 minutes with a lithium electrode already show chain scission presumably due to the reaction mechanism described in Equation 2 [49]. However, at the higher concentrations of wax, 6 and 8%, the resistance of the SEI was smaller than the unprotected pure PEO.

Fig. 17a is ac impedance data after two days of exposure to lithium metal. After two days, the low frequency semicircular feature has grown for all samples. This is especially the case for the pure PEO where, as described in previous work by Bruce [47,48] and seen in data presented here, the interfacial resistance of the SEI is larger than the resistance of the bulk polymer electrolyte. As the wax concentration is increased in the polymer electrolyte, the interfacial resistance is seen to decrease with respect to the pure PEO electrolyte. For the 6 and 8% films, the interfacial resistance is now less than the bulk polymer electrolyte value, a much more desirable condition. This indicates that the addition of the wax is providing stabilization of the SEI layer for extended periods of time.

Interestingly, the bulk polymer resistance is seen to decrease with the addition of the wax (Fig. 1). This has been observed before when additives of all types have been added to PEO electrolyte [72-74, 76] and has been suggested to be due to the change of crystallinity resulting from the addition of the additive.

ATR Infrared Spectroscopy data provides some insight into what is happening at the surface of the films before coming in contact with lithium metal. The ATR technique examines the surface of the film, which for the spectral region investigated goes to a depth of approximately 1 μm [49-51]. Fig. 18 is ATR FTIR data for the spectral region between 710 and 740 cm^{-1} where CH_2 rocking modes should occur. The rocking modes for $(CH_2)_4$ and longer hydrocarbon chains that are aligned and crystalline in nature are known to ‘‘split,’’ due to the crystal field effect, into two peaks appearing at approximately 720 and 730 cm^{-1} [79]. For shorter chains, and amorphous chain configurations, a single peak at approximately 720 cm-1 is seen. The spectrum for the pure PEO has no peaks in this region as one would expect, since there is no wax molecules with long chain hydrocarbon tails present. The film with 2% wax has a very slight indication of a mode close to 720 cm^{-1}. This mode becomes slightly stronger for the 4% system with perhaps the slight indication of a 730 mode. When 6 and 8% wax concentrations are reached, two modes are observed at 720 and 730 cm^{-1}. The observation of crystal field splitting indicates that there are CH_2 chains on the surface now aligned, forming self-assembled crystalline regions. It must be assumed that molecules “bloom” to the surface because of differences between bulk and surface free energies during removal of the solvent as the film is formed. It is most likely this same type of movement of additives to an interface in other polymer electrolytes results in their stabilization properties [61, 75, 76]. Additional evidence for the molecular layer at the polymer surface using AFM phase imaging will be

discussed later. This analysis correlates well with the ac impedance data. More wax on the surface, and wax where the very nonreactive hydrocarbon tails have assembled into crystalline surface layers, would be expected to better protect against reactions with lithium metal. At the lower concentrations of wax, there appears to not be a high enough concentration to form crystalline, more protective regions, again as shown by ac impedance data (Fig. 17).

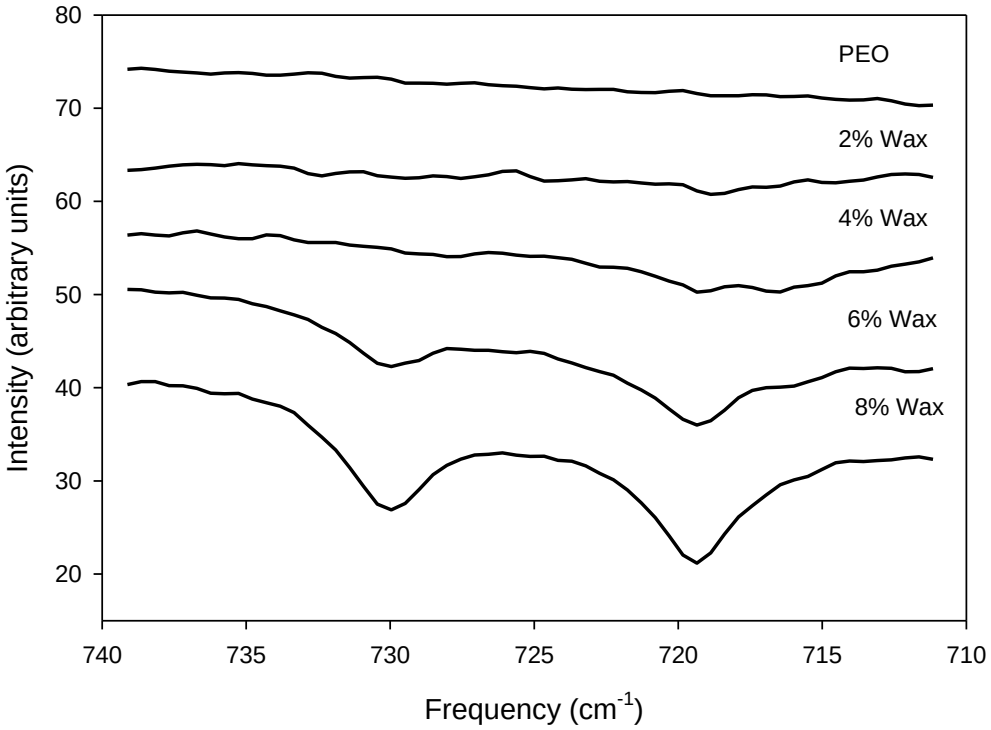

Fig.18. ATR FTIR spectra for the CH_2 rocking mode region. As the concentration of wax increases at the surface, crystal field splitting results in two modes at approximately 720 and 730 cm^{-1}, showing aligned, crystalline CH_2 chains at the surface.

Atomic force microscopy, and especially phase imaging, lends more information concerning the surfaces of the polymer electrolyte films. Phase imaging can be understood by first consider the tapping mode for AFM image collection. The cantilever is excited into resonance oscillation with a piezoelectric driver and the oscillation amplitude is used as a feedback signal to measure topographic variations of the sample. In phase imaging, the phase lag of the cantilever oscillations φ, measured relative to the drive signal oscillations, is simultaneously monitored. The phase lag recorded still has the high special resolution associated with AFM, but is also very sensitive to variations in material properties such as adhesion and viscoelasticity and can provide very valuable information concerning polymer surfaces.

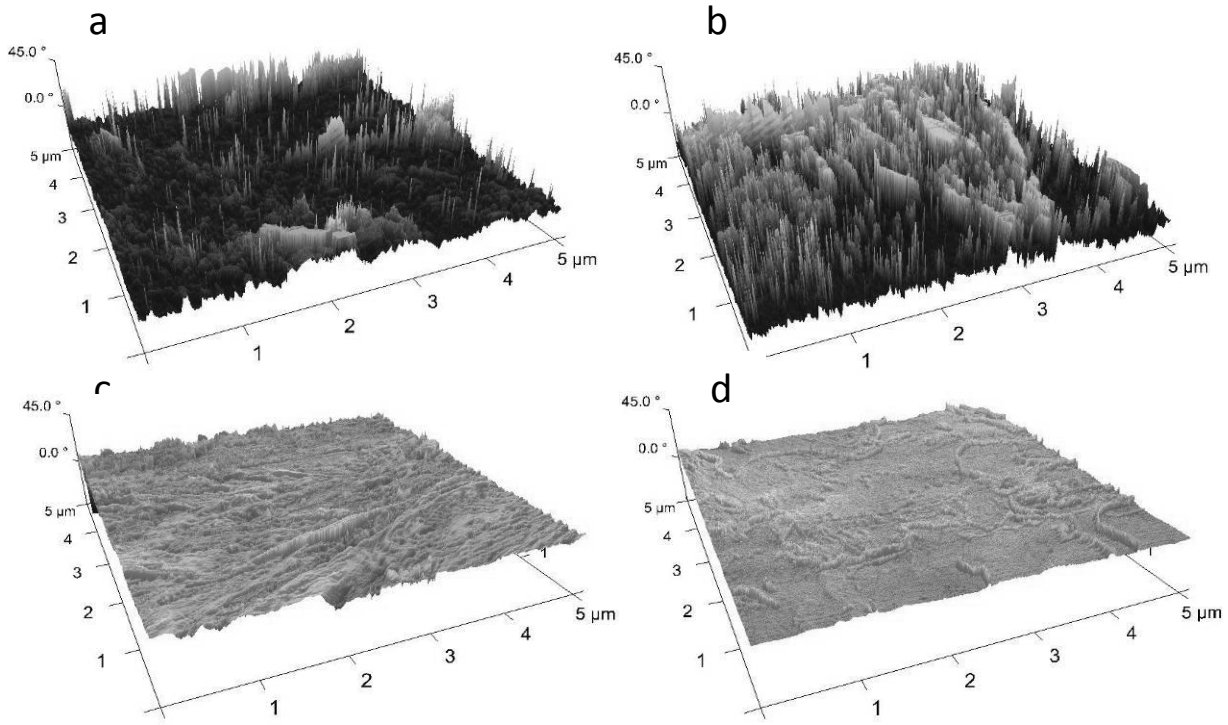

Fig. 19. AFM phase images of PEO electrolyte surfaces for polymer films with (a) no wax, (b) 2% wax, (c) 4% wax, and (d) 6% wax.

Phase images for the polymer electrolyte films with and without waxes are shown in Fig. 19. Fig. 19a is the phase image for the pure PEO. The very dark regions have a negative phase value, which indicates that the tip is very attracted to the polymer surface. This can be related to the amorphous regions of the heterogeneous PEO polymer where a large tip surface attraction would be expected. The light areas have a more positive phase value. These are attributed to crystalline regions on the pure PEO surface where interaction with the tip would be reduced due to the "hard" nature of the crystalline regions. Other AFM studies have seen the amorphous and crystalline areas on the surface of PEO electrolyte films [80, 81]; thus, it seems reasonable that this is what is being observed here. Fig. 19b is the phase image of the 2% wax film. Here many bright regions can be seen though they appear to be very dispersed in nature. These are postulated to represent the hydrocarbon chains that have bloomed to the surface. The tip does would not have strong interactions with the hydrocarbon chains and the phase is therefore more positive. The dispersed nature of the hydrocarbon correlates with the ATR FTIR data. The IR spectrum for the 2% wax indicates that the CH2 chains are not coalesced enough to form crystalline regions as suggested by AFM phase data. Fig. 19c is for the 4% wax PEO surface. In general, the surface has a very positive phase interaction; however, it still appears to be very uneven in nature. This again correlates with IR data in that a slight indication of crystallinity is shown in the IR data. Fig. 19d is for the 6% wax film. Here the surface has a very highly uniform and low interaction with the tip, indicative of the positive phase values. The IR data shows that at these concentrations the surface CH_2 chains are in a highly ordered crystalline state, which is the type of surface shown in Fig. 19d. The phase image for the 8% wax film is very similar to the 6%, as would be expected from the IR data, and is not shown. AC impedance data corroborates these observations. At concentrations of 6 and 8%, the maximum stabilization

of the interface is achieved (Fig. 11). At the 2% concentration, the interfacial impedance grows with time, much like the unprotected PEO electrolyte film. Fig. 3b shows that the 2% film, while having longer hydrocarbon chains on the surface, does not have a high enough concentration of the wax to coalesce into crystalline layers with the maximum resistance to lithium reactions.

V.D. Conclusions

A simpler method for placing protective layers at the surface of polymer electrolyte was described. It consisted of a single step film casting technique where the electrolyte films are prepared by casting a solution composed of the PEO polymer electrolyte, inorganic salt and the molecules that form the self-assembled layers on the surface of the polymer electrolyte. The molecules forming the self-assembling monolayer "bloomed" to the surface during removal of the solvent as the film is formed because of the difference in free energies between the forming bulk film and its surface. These molecular layers stabilized the SEI layer formed between lithium metal and the polymer electrolyte and, at a level of 6% and above, there was significant interfacial stabilization. Below these levels, there were not sufficient hydrocarbon chains to form a complete, aligned, crystalline layer necessary for SEI stabilization. The structure of the protective film at the surface was investigated by ATR FTIR spectroscopy and AFM phase imaging. The phase images were found to be an excellent way of looking at the coverage of the polymer electrolyte surface for determining whether the film had good coverage by the protective monolayer, or whether it was too dispersed to form a useful layer of protection again lithium. Interesting questions remain. While the molecular protective layer protects against unwanted lithium reactions, the ions appear to be able to move easily through this layer. Ion conduction through these protective layers has been observed for other monolayer films on polymer electrolytes [49-51, 77, 78], but how lithium ions can move readily through a hydrophobic hydrocarbon layer has yet to be determined. This will be the object of future studies.

VI. The fabrication and characterization of electrolyte systems confined in nanoporous membranes for electrolytes with enhanced performance.

V.I.A. Introduction

Poly(ethylene oxide), PEO, complexed with inorganic salts, has been the object of intense study as a solid electrolyte material. PEO's low Tg, facilitates backbone motion for good plasticity at room temperature, but yet has a sufficient modulus to prevent lithium dendrite growth. Its relatively high dielectric constant promoting ion disassociation makes it an interesting material for a solid electrolyte. However, for practical application, the ionic conduction through a polymer electrolyte must approach 10^{-3} Scm^{-1} at room temperature [82] as compared to a typical value for polymer electrolyte composed of only salt and the PEO polymer of from 10^{-7} to 10^{-8} Scm^{-1}. Thus, work on enhancing ion conduction for PEO polymer electrolytes has received much attention. While gel polymer electrolytes containing additional liquid such as propylene carbonate or ethylene carbonate have enhanced ion conduction, they cause the polymer to lose mechanical properties and can promote the formation of an unstable

passivation layer at the lithium/polymer electrolyte interface [82]. Other methods for improving ion conduction in polymer electrolytes have been investigated. These include the use of flexible backbone polymers like polysiloxanes and polyphosphazenes that have side chains of PEO polymer [83] where the flexibility of the polymer backbone promotes segmental motion, thereby increasing ion conduction. The addition of micro and nanoparticles (nanofillers) of insulating inorganic materials, such as Al_2O_3, SiO_2, $LiAlO_2$, zeolites, and the addition of organic particles, such as polyacrylamide, to polymer electrolytes have been found to increase ion conduction [84-93]. These fillers increase conduction by mainly decreasing crystalinity in the polymer electrolyte [94]. Conducting fillers such as β-alumina, Li_3N, $LiAlO_2$ and others have also been studied [95-102]. Recent work involving enhanced ion conduction in polymer electrolytes has involved the alignment of conducting regions in the polymer and confinement in channels or phase regions. Alignment of the polymer electrolyte backbone by stretching [103-105] or by using magnetic fields[106-108] have been found to increase ionic conduction by 4 to 40-fold. Dang et al. [109] have seen anisotropic ionic conduction in rigid rod, liquid-crystalline polymers while studies have been conducted on the ionic conductivity of liquid crystal, smectic phase polymer electrolytes [110-112] and on alkali salts incorporated in the oligoethoxy chains located in the central channels of columnar mesophases [113, 114].

An interesting area of work has investigated the use of interpenetrating networks where one phase is the ion conducting phase while the other non-conducting phase can provide mechanical reinforcement that promotes the dimensional stability of the formed polymer electrolyte composite [115-131]. In many cases, the non-conducting phase appears to enhance conduction [117, 118, 126, 127, 131] as is observed for micro and nanoscale filler materials. Recent work has involved PEO-complex polymer electrolyte confined in the nanopores of structurally well-defined membranes having channels that are parallel to each other and are perpendicular to the surface of the membrane [94, 117, 126-128, 131]. This channel geometry is intriguing for several reasons. First, ion conduction of the polymer electrolyte appears to be increased upon this confinement. The reason for this increased ion conduction has been attributed to many factors, including enhanced conduction associated with the interface between the polymer electrolyte and the nonconducting channel phase, the orientation effects of amorphous and crystalline regions in polymer electrolytes resulting from the confined conditions and effects on the glass transition, and crystallinity and diffusional dynamics, since confinement is known to affect these properties of polymers [132]. In addition, the enhanced ion conduction in these polymer composite electrolyte membranes is facilitated along the long axis of the channels, i.e. perpendicular to the membrane surface. This is the desired configuration for battery fabrication with the ions moving easily through the polymer electrolyte composite membrane between the anode and cathode.

This work investigates an interpenetrating network structure where “tubes” of polymer electrolyte are placed in the nanopores of anodic aluminum oxide (AAO) membranes. These systems have interesting ion conduction properties that will be discussed.

VI.B. Experimental

Preparation of the AAO PEO complex membranes has been described previously [127]. As before, PEO with a molecular weight of 4,000,000 (Aldrich) and lithium triflate ($LiSO_3CF_3$, Aldrich) was dissolved in Optima grade acetonitrile (Fisher) at an ether oxygen to lithium ion ratio of 15:1. Nanoporous AAO membranes were obtained from Whitman. These membranes provide the rigid nonconducting structure that have well ordered channels into which the PEO polymer electrolyte can be deposited. Filling pores of this size can be difficult and this process was facilitated by a new technique of placing the membranes in a filtration membrane holder attached to a syringe. By expelling the solution in the syringe, the electrolyte solution was "pushed" through the membrane pores, filling them with polymer electrolyte solution. Capillary action kept the solution in the membranes while they were removed from the holder, and placed in a Teflon container where they were covered with the PEO/lithium triflate solution. The solvent was removed by placing the containers in a glass desiccation jar with N_2 flowing through the system. In this manner, the solvent was evaporated, leaving the polymer films that contained the alumina membranes and forming the polymer electrolyte/membrane composite. Fig. 20 shows AAO membranes contained in the resulting polymer films. The volume of solution placed over the membranes could be adjusted so that the thickness of the polymer surrounding the membrane could be varied. The ability to change the thickness of the film surrounding the AAO membrane will prove to be useful for understanding these systems.

Fig. 20 PEO electrolyte film containing AAO Membrane

AC Impedance data were collected with a Solartron 1260 impedance/gain-phase analyzer with 1296 dielectric interface. The frequency used for testing was between 1×10^6 to 0.01Hz at a fixed ac level of 500 mV. Impedance data were collected by placing the composite membranes between two stainless steel disks held at a constant force by a cell holder and all measurements were made in an argon atmosphere glovebox. DSC experiments were made by using a Mettler DSC 822e. The membranes were cut into small sections and placed in standard aluminum DSC pans. The thermograms were corrected for weight so that direct comparisons could be made between samples of varying weight. Data were measured from −90 to 100 °C at 10°C/min, using liquid N_2 as the cooling medium. Scanning electron microscope images were collected using a FEI Helios 600 system. Cross-sectional membrane surfaces for SEM images were obtained by

placing the composite membranes containing the polymer electrolyte in liquid nitrogen, lowering the polymer temperature below its glass transition temperature, and then breaking the membranes. This exposed the cross-section desired for SEM investigation.

VI.C. Results and Discussion

The evaporation of the solvent as the film was formed resulted in an interesting structure. The pores in the alumina instead of being filled with polymer electrolyte became coated with a "sleeve" of polymer. This composite structure is shown schematically Fig. 21a. Below the schematic are two SEM cross-sectional images where the tubes lining the channels in the membranes can be seen. In Fig 21b the membrane is fractured and the sleeves of polymer can be seen pulling out of the membrane while in Fig. 21c, polymer sleeves protruding from the edge of the membrane are exposed. The approximate thickness of these tubes was determined to be 10 nm.

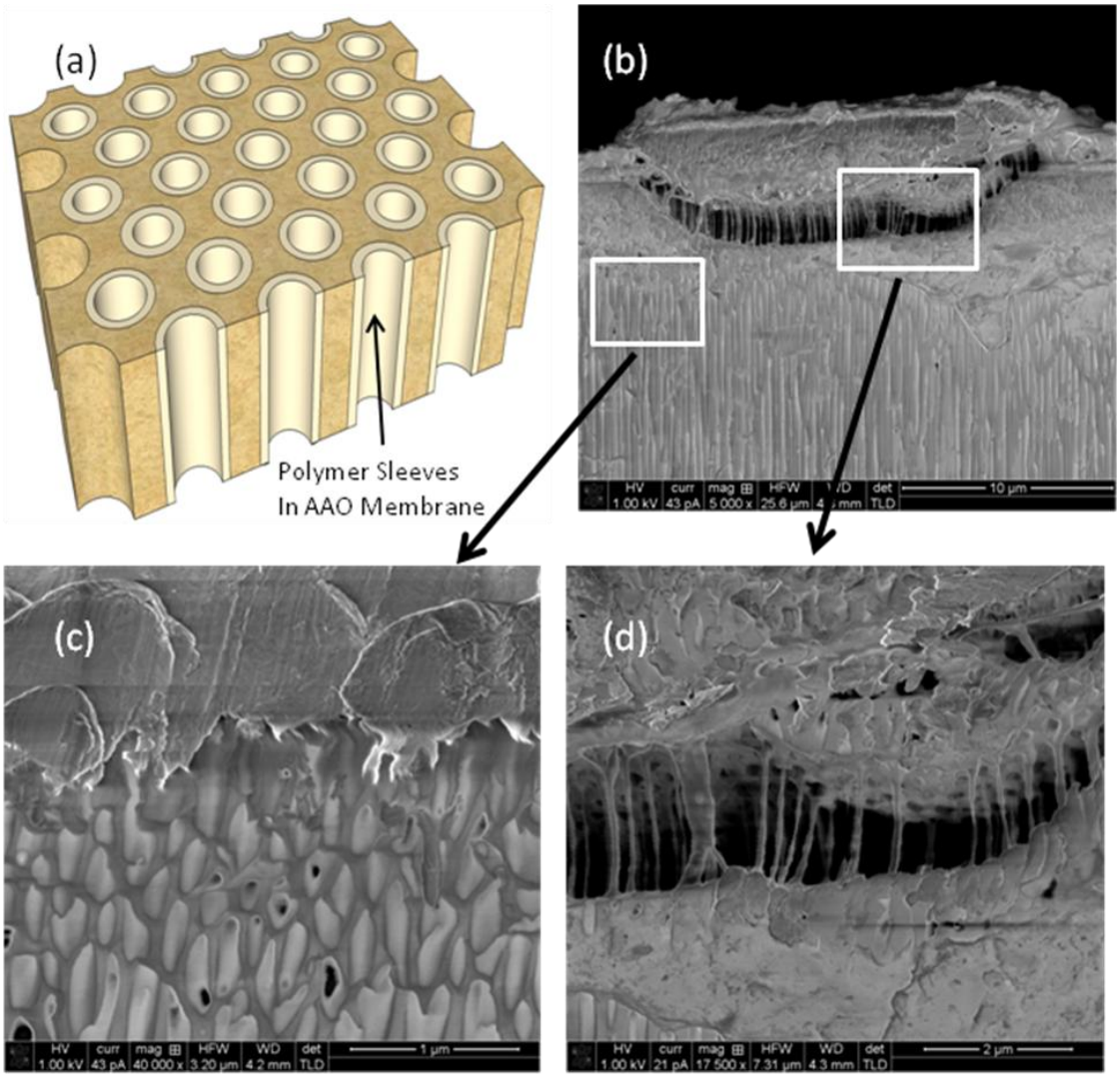

Fig. 21. (a) diagram of polymer sleeves in AAO membrane. (b) SEM cross-sectional images of AAO membrane containing PEO polymer electrolyte (c) higher magnification showing oblique fracture where polymer tubes with some openings shown (d) higher magnification showing membrane separation, tubes can be seen stretched Between separation.

During fabrication of the composite membranes, and as described earlier in the experimental section, the volume of solution placed over the membranes could be adjusted so that when the solvent was removed by evaporation, the thickness of the polymer surrounding the membrane could be varied. Composite membranes with only a very thin covering of polymer electrolyte could be fabricated. AC impedance data collected through these samples would be due to both the film covering the membranes and the tubes extending completely through. However, since very thin polymer films that encase the membrane could be fabricated, ac impedance data collected on these membranes covered with a very thin layer of polymer, where the length of the tubes in the membranes is much longer than the thin film surrounding it, the observed ion conduction must be considered to originate mainly from ion conduction through the tubes.

AC impedance data were collected for two types of systems. The first was the composite membranes/PEO as described above. The second was collected from a section of the polymer film next to the membrane, but not containing the AAO membrane (see Fig. 20). These latter films served as excellent standards for comparison, since they came from the same films formed from casting and evaporation of the solvents and, of course, would have the same thickness as the membranes/PEO films incased in polymer electrolyte. AC impedance data are shown in Fig. 22 where data for the polymer composite membranes and for the pure polymer are shown. Considering the polymer ion conduction to be described by an equivalent circuit composed of a capacitor and resistor in parallel, the resistance of the two samples can be estimated by the intersection of the semicircular feature of the data with the x axis. Interestingly, the AAO composite membrane has a slightly higher conduction than pure polymer film. However, in order to make valid comparisons, specific resistance values were calculated. Assuming all of the pores were full (which SEM images indicate), knowing the diameters of the pores, the thickness of the sleeves, length of the sleeves and pore density, one can calculate a specific conductivity for the confined polymer. These data can be compared to the polymer not containing an AAO membrane. The standard film had a specific conductivity of 9 x 10^{-9} Ω^{-1} cm^{-1}. while the confined film had a value of 4 x 10^{-7} Ω^{-1} cm^{-1}. This is an increase by a factor of over 40 for the ion conduction through the sleeves of the tube compared to a standard PEO film. The increase in conduction upon

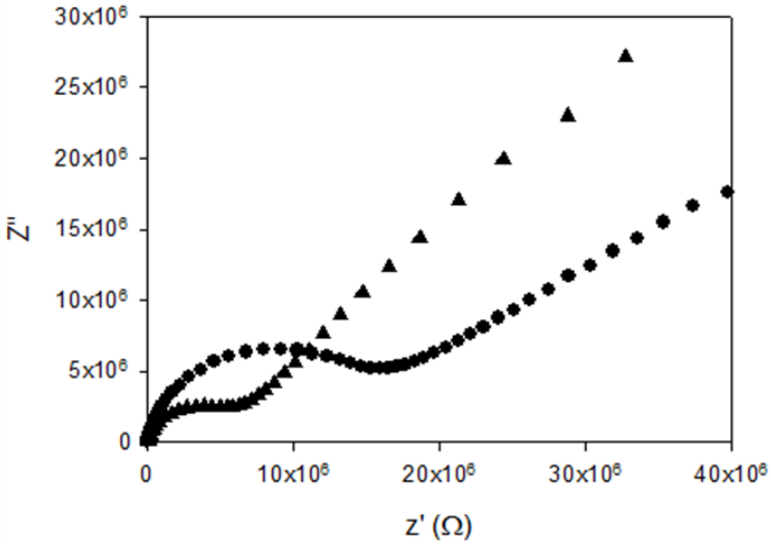

Fig. 22. Nyquist plots for PEO confined in nanoporous AAO membrane (▲) and non-confined PEO (●)

confinement is comparable to the enhancement in ion conduction seen for some PEO-complexed films that have been mechanically stretched [103, 105] and those aligned by magnetic field [106-108].

What could be happening to increase the ion conduction? Thermal Analysis data can help with this question. Fig. 23 shows DSC data for a membrane that is encased in relative thin coating of polymer (23a) and a thermogram for one that has relatively thick coating of polymer surrounding the membrane (23b). The corresponding SEM images of the composite membranes associated with these themograns are shown to the right of the DSC thermograns. In the former, thermogram (23a), one would expect to see a thermal contribution mostly from the polymer confined in the membrane while in the latter case, thermogram (23b), one could expect to see a contribution from the polymer in the tubes and, if different in nature, a contribution from the PEO film covering the AAO membrane. The PEO for just the sleeves shows a broad endothermic peak that must be associated with the PEO electrolyte from the tubes. When extra PEO is present, an additional, sharper peak is seen that must be associated with the polymer film surrounding the membrane, which is not confined. With this assignment for the endotherms in the thermogram, the melting temperature of the non-confined PEO electrolyte is seen to be approximately 67°C while the broad endotherm associated with the melting temperature for the sleeves of polymer is located at 47 °C. These data correlate with studies performed by Lagrene and Zanotti and our work on PEO complexes confined in AAO channels [127, 133] where the crystal melting temperature decreased compared to non-confined PEO complexes.

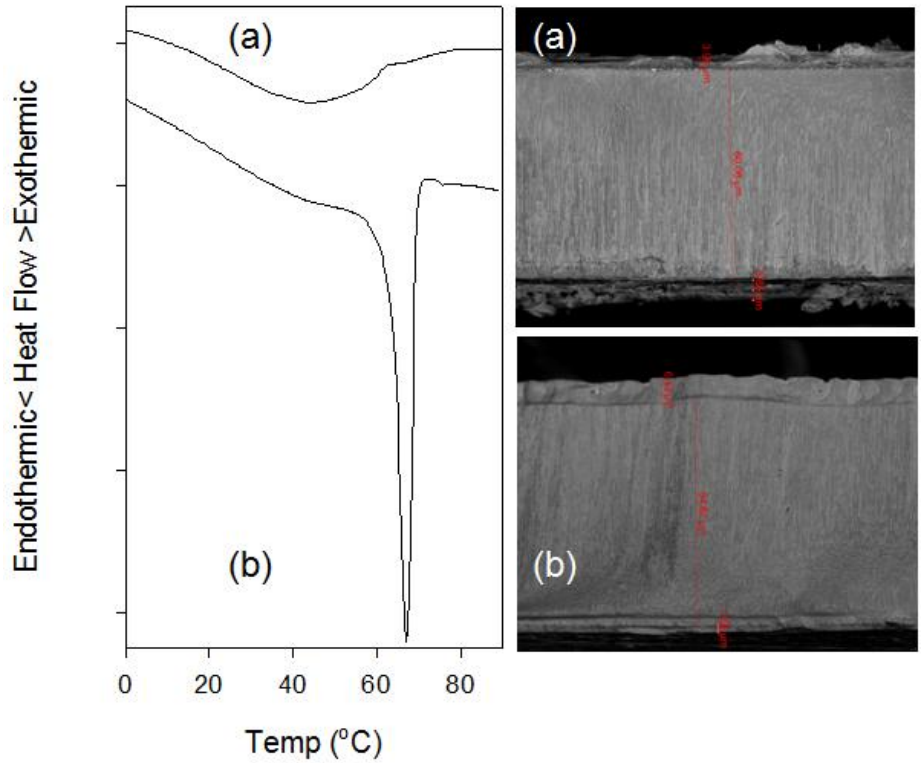

Fig. 23. DSC thermograms (left) and SEM cross-sectional images for the corresponding PEO electrolyte in AAO membrane (right). Data (a) are for membranes contained in very thin films while (b) is covered with a thicker film.

Thermal analysis data indicates that the polymer film in the pores has a different crystalline nature with a possible broader crystallite size distribution than that of the non-confinded PEO. Our previous studies have shown similar behavior for confined polymer electrolytes [127]. Investigating this issue can be addressed by calculating the crystallite thickness l_c for the pure PEO electrolyte and the electrolyte in the membrane, which can be done by using the Thomson-Gibbs equation [134]

$$T_m^{tr} = T_m^o \left(1 - \frac{2\gamma_i}{\Delta H_m^o \rho_c l_c}\right) \qquad (10)$$

where T_m^{tr} is the observed melting temperature, T_m^o is the equilibrium melting temperature of PEO crystallites (69°C [135]), ΔH_m^o = 197 J/g and is the enthalpy of melting of a perfect crystal of PEO [135], ρ_c is the density of PEO crystals which is 1.3 g/cm^3 and γ_i is the free surface energy of the faces at which the PEO chains fold into lamella that ≅ 3 x 10^{-6} J/cm^2 [136]. The calculated values of crystallite thickness for the non-comfined PEO is found to be 40 nm while that for the confined is 7 nm.

The smaller crystallite thickness could help to explain the enhanced ion conduction observed for the polymer sleeves. Smaller crystallites may result in more grain boundaries in the polymer where enhanced conduction could occur [94]. Smaller crystallites could also mean a more open structure with room for amorphous material between the crystallites in the polymer matrix, i.e. less crystallinity. Amorphous material is generally accepted as having much higher ion conduction than crystalline regions; thus, the more amorphous mature of the sleeves would promote ion conduction.

A more detailed consideration of the amorphous regions can be made and this can lend to additional understanding of increased conduction. Schönhals et al. conducted dielectric spectroscopy studies on polymer chains of polyethers confined in pores and determined that the chains are stretched relative to non-confined PEO [132]. Modeling for PEO amorphous systems has indicated that stretching of the backbone results in the unraveling of loops, a resultant increase in order in the polymer chains, and increased conduction [137]. Stretching of the polymer backbones in the amorphous regions of the PEO trapped in the nanopores of the membranes would promote enhancing conduction. It is very possible that a combination of less crystallinity and better alignment of the polymer backbones in the amorphous phase could promote ionic conduction.

VI.D. Conclusions

A novel polymer electrolyte nanostructure consisting of PEO polymer in the form of sleeves or tubes approximately 10nm in thickness in 200 nm pores of AAO membranes was fabricated. The confinement of the electrolyte in this nanostructure increased the ion conduction of the polymer by over 40 orders of magnitude. Thermal analysis data exhibited a broad endotherm for the confined PEO while non-confined PEO polymer electrolyte had a melt

endotherm that was much sharper. The melting temperature for the confined PEO was lowered to 47°C compared to a melting temperature of 67°C for the non-confined PEO. These data correlate well with previous research that shows a reduction in the melting temperature of PEO polymer confined in pores [127]. Analysis of these melting temperature shows that the crystallite thickness for the confined PEO is much smaller than non-confined PEO. These smaller crystallites could result in a more amorphous phase being present in the polymer matrix contributing to the enhanced ion conduction [132]. In addition, the confinement of polyethers in pores is known to result in stretching and ordering of the backbone [132], which has been postulated to increase ion conduction [137]. The presence of more amorphous polymer and ordering of the backbone would seem to be the major factor involved in the enhancement of ion conduction observed. Further work will study the relative contribution of reduction in crystallinity and backbone ordering to enhanced ion conduction in the composite system. Studies will be augmented by having pores with different diameters where the effect of tube diameter on ion conduction can be investigated.

VII. Integration of nanostructured and nanoengineered technologies into battery systems for maximum battery performance.

Activities conducted on battery materials using nanotechnology techniques are described in previous sections in this report. Possible ways of integrating components together to fabricate batteries that integrate the technologies described in this report will be briefly discussed in this section.

A potential battery design is shown in Figs. 24 and 25. AAO membranes serve as the foundation for much of the work described in this report and will serve as the foundation for a potential battery design described here. Fig.24a shows a typical sized AAO membrane available commercially, such as those from Whatman or Synkera. This would serve as the substrate for the growth of nanostructured electrodes,as described in Section III, by a sputter coating process. The image of this "nanobasket" structure is shown again in Fig. 24b. At this point, the nanobaskets in this structure would be individually wired with a nanowire as described in Section IV. An actual SEM image of nanowires, running through the alumina membrane, coming in contact with the electrode nanobasket nanostructured, is shown in Fig. 24c. An illustration of the complete integrated electrode configuration is shown in the lower left of Fig. 24 where the nanowires inside the AAO channels, extending into the nanobasket, are visible. The opposite ends of the nanowires, the end where they would exit from the AAO membranes, would be where common contacts with all the nanobasket structure could be made. This common contact would thus make sure that all the electrode material has intimate contact with the current collector by taking advantage of the electrode's nanostructure. The second battery electrode could be fabricated in a similar manner. Thus, a nanostructured anode and cathode with a nanowire current collector would be fabricated.

For the next part of construction of the battery containing integrated nanoengineered features, polymer electrolyte would be used. Both a lithium ion configuration and a lithium metal polymer battery could be considered. For the lithium ion battery, the electrolyte materials could be liquid or solids such as polymeric electrolyte. These electrolytes could take advantage

of factors discussed in prior sections of this work. For a lithium ion polymer electrolyte system, a thin polymer film would be placed between an anode and a cathode nanostructured electrode/current collector system. A film casting process with a final melting of the film would be used to assemble the anode and cathode together into a complete battery, Fig.25a and 25b. The melting would allow the electrolyte to move into the crevices of the tops of the nanobasket structure (Fig. 24d) where the confined nature of the electrolyte would be able to provide the increased ion conduction described in Section VI.

Lithium metal polymer batteries would have only the cathode in the nanowired, nanostructured configuration. A polymer electrolyte would be used again, with lithium metal used as the anode (Fig.25 b). To stabilize the lithium metal/polymer electrolyte interface, the polymer electrolyte will have the surfactant described in Section V that can bloom to the surface of the electrolyte, forming a stabilizing layer at this interface.

These complete batteries could be incased for protection (Fig.25c) and finally folded (Figs.25d and 25e) to make more compact packs of batteries.

Fig. 24

Fig. 24d. Looking at the surface of the nanobasket structure. Crevices in the structure provides area where the polymer electrolyte can penetrate. This confinement enhances ion

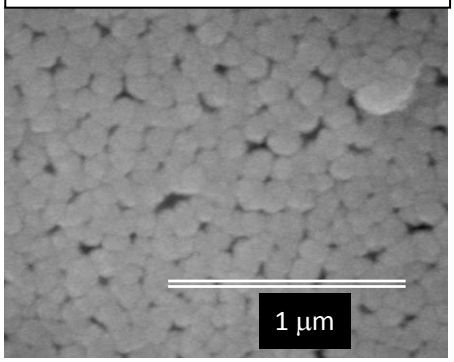

Fig. 24 a. AAO nanoporous membrane that serves as the foundation upon which much of the battery nanostructure is based.

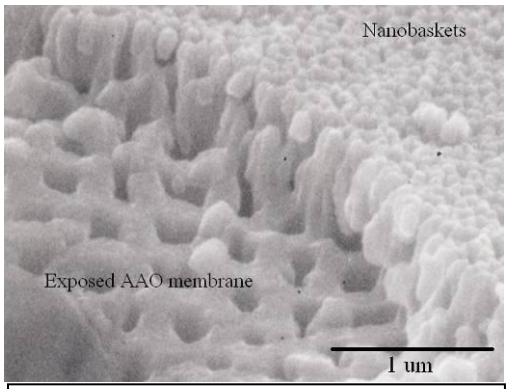

Fig. 24b. Nanobaskets on top of AAO nanaporous membrane

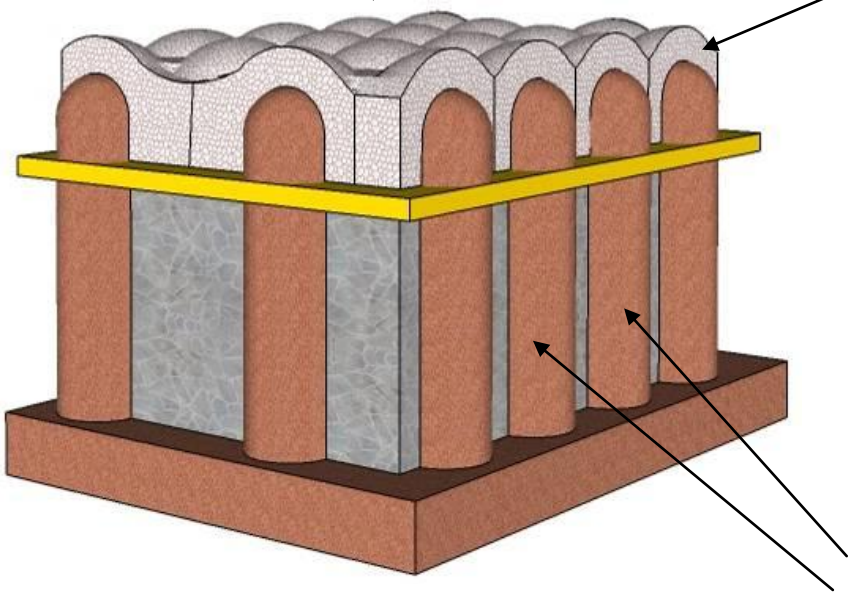

Integrated Electrode System.

Fig. 24c. Current-collecting nanowires going through AAO membrane pores to make contact with electrode nanobasket nanostructure.

Fig. 25

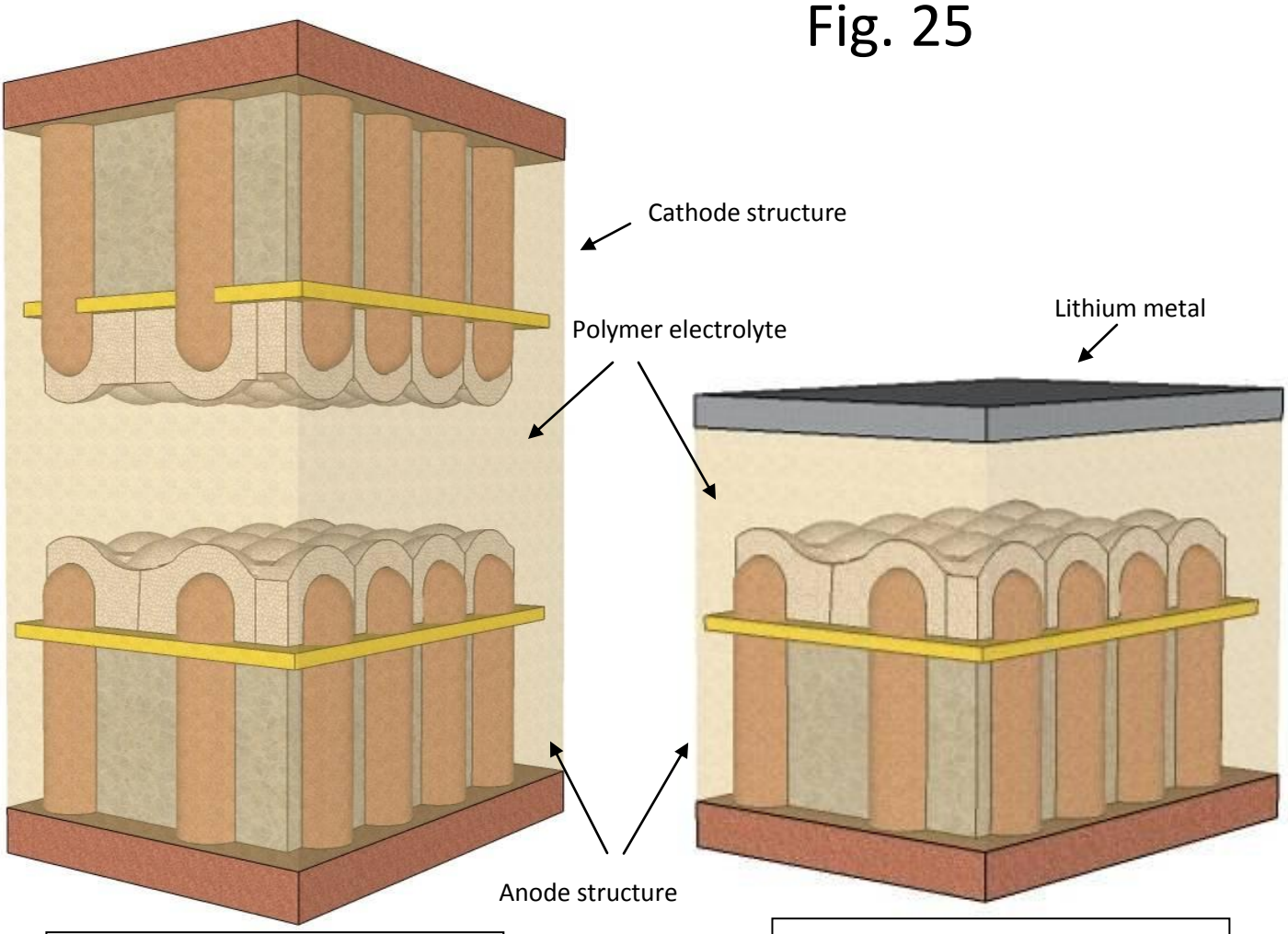

Fig. 25a. Lithium ion configuration with polymer electrolyte.

Fig. 25b. Lithium meta polymer electrolyte configuration with polymer electrolyte.

Fig. 25d

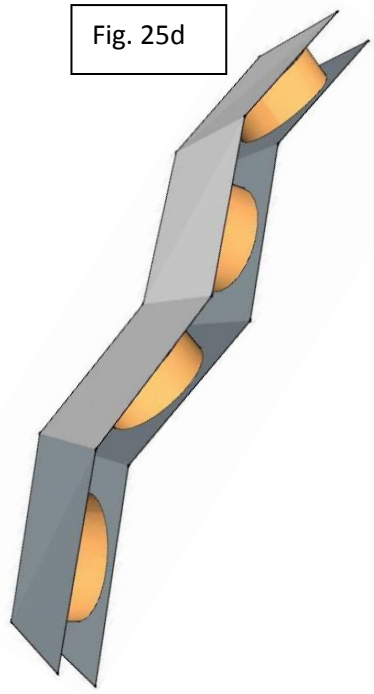

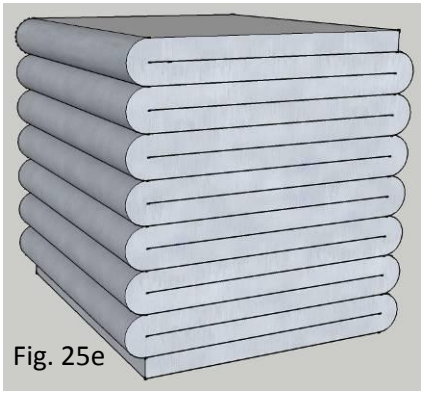

VII. References

[1]. T.J. Kim, D. Son, J. Cho, B. Park, H. Yang, *Electrochimica Acta*, **49**, 4405-4410 (2004).

[2]. S.T. Chang, I.C. Leo, C.L. Liao, J.H. Yen, M.H. Hon, *Journal of Materials Chemistry*, **14**, 1821-1826 (2004).

[3]. C. Jiang, E. Hosono, H. Zhou, *Nano Today*, **1**, 28-33 (2006).

[4]. H. Zhou, D. Li, M. Hibino, I. Honma, *Angewandte Chemie International Edition*, **44**, 797-802 (2005).

[5]. L.Y. Beaulieu, K.W. Eberman, R.L. Turner, L.J. Krause, J.R. Dahna, *Electrochemical and Solid-State Letters*, **4**, A137-A140 (2001).

[6]. F. Robert, P.E. Lippens, J. Olivier-Fourcade, J.C. Jumas, F. Gillot, M. Morcrette, J.M. Tarascon, *Journal of Solid State Chemistry*, **180**, 339-348 (2007).

[7]. C.H. Ko, H.I. Song, S.S. Han, S.H. Cho, J.N. Kim, in: AIChE Annual Meeting, Conference Proceedings, 2005, pp. 11176.

[8]. S.T. Chang, I.C. Leu, M.H. Hon, *Electrochemical and Solid-State Letters*, **5**, C71-C74 (2002).

[9]. J.P. Maranchi, A.F. Hepp, P.N. Kumta, *Materials Science and Engineering B: Solid-State Materials for Advanced Technology*, **116**, 327-340 (2005).

[10]. M. Mohamedi, S.J. Lee, D. Takahashi, M. Nishizawa, T. Itoh, I. Uchida, *Electrochimica Acta*, **46**, 1161-1168 (2001).

[11]. Y.D. Ko, J.G. Kang, J.G. Park, S. Lee, D.W. Kim, *Nanotechnology*, **20**, (2009).

[12]. L.K. Hutter, P.L. Johnson, D. Teeters, in: ACS National Meeting Book of Abstracts, 2007.

[13]. P.L. Johnson, D. Teeters, *Solid State Ionics*, **177**, 2821-2825 (2006).

[14]. G. Taillades, N. Benjelloun, J. Sarradin, M. Ribes, *Solid State Ionics*, **152-153**, 119-124 (2002).

[15]. M. Smith, P Johnson, D. Teeters, Solid State Ionics, 2012, In Press.

[16]. J. Jamnik, J. Maier, *Physical Chemistry Chemical Physics*, **5**, 5215-5220 (2003).

[17]. E.A. Kotomin, Y.F. Zhukovskii, P. Balaya, J. Maier, in: 213th ECS meeting Abstracts 2008, 2008, pp. 414.

[18]. J. Maier, *Journal of Power Sources*, **174**, 569-574 (2007).

[19]. J. Maier, *Faraday Discussions*, **134**, 51-66 (2007).

[20]. Y.F. Zhukovskii, P. Balaya, E.A. Kotomin, J. Maier, *Physical Review Letters*, **96**, (2006).

[21]. C.K. Chan, H. Peng, G. Liu, K. McIlwrath, X.F. Zhang, R.A. Huggins, Y. Cui, Nat. Nanotechnol. 3 (2008) 31.

[22]. R. W. Hart, H. S. White, B. Dunn, D. R. Rolison, Electrochem. Commun. , 5 (2003) 120-123.

[23]. W. Long Jeffrey, B. Dunn, R. Rolison Debra, S. White Henry, Chem Rev 104 (2004) 4463-4492.

[24]. P. L. Taberna, S. Mitra, P. Poizot, P. Simon, J. M. Tarascon, Nat. Mater. , 5 (2006) 567-573.

[25]. A. Singh, J. Jayaram, M. Madou, S. Akbar, J. Electrochem. Soc. , 149 (2002) E78-E83.

[26]. M. Nathan, D. Golodnitsky, V. Yufit, E. Strauss, T. Ripenbein, I. Shechtman, S. Menkin, E. Peled, J. Microelectromech. Syst., 14 (2005) 879-885.

[27]. D. Golodnitsky, M. Nathan, V. Yufit, E. Strauss, K. Freedman, L. Burstein, A. Gladkich, E. Peled, Solid State Ionics 177 (2006) 2811-2819.
[28]. J. O. Besenhard, J. Yang, M. Winter, J. Power Sources 68 (1997) 87-90.
[29]. I. A. Courtney, J. R. Dahn, J. Electrochem. Soc., 144 (1997) 2045-2052.
[30]. J. S. Sakamoto, C. K. Huang, S. Surampudi, M. Smart, J. Wolfenstine, Mater. Lett., 33 (1998) 327-329.
[31]. B. Wu, J. J. Boland, J. Colloid Interface Sci. , 303 (2006) 611-616.
[32]. T. Gao, G. W. Meng, J. Zhang, Y. W. Wang, C. H. Liang, J. C. Fan, L. D. Zhang, Appl. Phys. A: Mater. Sci. Process. , 73 (2001) 251-254.
[33]. W. Steinhogl, G. Schindler, G. Steinlesberger, M. Traving, M. Engelhardt, J. Appl. Phys. , 97 (2005) 023706/023701-023706/023707.
[34]. K. Hinode, Y. Hanaoka, K.-I. Takeda, S. Kondo, Jpn. J. Appl. Phys., Part 2 40 (2001) L1097-L1099.
[35]. H. H. Wang, C. Y. Han, G. A. Willing, Z. Xiao, Mater. Res. Soc. Symp. Proc., 775 (2003) 107-112.
[36]. L. L. Diaz-Flores, R. Ramirez-Bon, A. Mendoza-Galvan, E. Prokhorov, J. Gonzalez-Hernandez, J. Phys. Chem. Solids 64 (2003) 1037-1042.
[37]. M.-S. Park, Y.-M. Kang, G.-X. Wang, S.-X. Dou, H.-K. Liu, Adv. Funct. Mater. , 18 (2008) 455-461
[38]. J. M. Tarascon, M. Armand, *Nature*, **414**, 359-67 (2001).
[39]. D. Aurbach, Y. Gofer, M. Ben-Zion, P. Aped, *J. Electroanal. Chem*., **339**, 451-71(1992).
[40]. D. Aurbach, I. Weissman, H. Yamin, E. Elster, *J. Electrochem. Soc*., **145**, 1421-1426 (1998).
[41]. D. Aurbach, E. Zinigrad, Y. Cohen, H. Teller, *Solid State Ionics*, **148**, 405-416 (2002).
[42]. J. O. Besenhard, G. Eichinger, *J. Electroanal. Chem. Interfacial Electrochem*., 68, 1-**18** (1976).
[43]. A. Teyssot, C. Belhomme, R. Bouchet, M. Rosso, S. Lascaud, M. Armand, *J. Electroanal. Chem*., **584**, 70-74 (2005).
[44]. D. Aurbach, Y. Cohen, *Electrochem. Solid-State Lett*., 2, 16-18 (1999).
[45]. Y. S. Cohen, Y. Cohen, D. Aurbach, *J. Phys. Chem. B*, **104**, 12282-12291 (2000).
[46]. J.-i. Yamaki, S.-i. Tobishima, K. Hayashi, K. Saito, Y. Nemoto, M. Arakawa, *J. Power Sources*, **74**, 219-227 (1998).
[47]. P. G. Bruce, F. Krok, *Electrochim. Acta*, **33**, 1669-74 (1988).
[48]. P. G. Bruce, F. Krok, *Solid State Ionics*, **36**, 171-4 (1989).
[49]. M. Le Granvalet-Mancini, T. Hanrath, D. Teeters, *Solid State Ionics*, **135**, 283-290 (2000).
[50]. M. Le Granvalet-Mancini, L. Honeycutt, D. Teeters, *Electrochimica Acta*, **45**, 1491-1500 (2000).
[51]. M. Le Granvalet-Mancini, D. Teeters, *Journal of Power Sources*, **97-98**, 624-627 (2001).
[52]. R. N. Mason, M. Smith, T. Andrews, D. Teeters, *Solid State Ionics*, **118**, 129-133 (1999).
[53]. Y. Malik, D. Aurbach, P. Dan, A. Meitav, *J. Electroanal. Chem*., **282**, 73-105 (1991).
[54]. P. Ravn Sørensen, T. Jacobsen, *Electrochim. Acta*, **27**, 1671-1675 (1982).
[55]. B. C. H. Steele, G. E. Lagos, P. C. Spurdens, C. Forsyth, A. D. Foord, *Solid State Ionics*, **9-10**, 391-398 (1983).
[56]. I. I. Olsen, J. Barker, R. Koksbang, *Solid State Ionics*, **83**, 125-133 (1996).

[57]. D. Fauteux, *Solid State Ionics*, **17**, 133-8 (1985).
[58]. M. Hiratani, K. Miyauchi, T. Kudo, *Solid State Ionics*, **28-30**, 1431-1435 (1988).
[59]. C. A. Vincent, *Progress in Solid State Chemistry*, **17**, 145-261 (1987).
[60]. N.-S. Choi, Y. M. Lee, W. Seol, J. A. Lee, J.-K. Park, *Solid State Ionics*, **172**, 19-24 (2004).
[61]. K. Naoi, M. Mori, M. Inoue, T. Wakabayashi, K. Yamauchi, *J. Electrochem. Soc*., **147**, 813-819 (2000).
[62]. C. Liebenow, K. Luehder, *J. Appl. Electrochem*., **26**, 689-692 (1996).
[63]. H. Ota, K. Shima, M. Ue, J.-i. Yamaki, *Electrochim. Acta*, **49**, 565-572 (2004).
[64]. H. Ota, Y. Sakata, Y. Otake, K. Shima, M. Ue, J.-i. Yamaki, *J. Electrochem. Soc*., **151**, A1778-A1788 (2004).
[65]. S. Shiraishi, K. Kanamura, Z. I. Takehara, *J. Appl. Electrochem*., **29**, 869-881 (1999).
[66]. K. M. Abraham, J. S. Foos, J. L. Goldman, *J. Electrochem. Soc*., **131**, 2197-9 (1984).
[67]. R. Mogi, M. Inaba, S.-K. Jeong, Y. Iriyama, T. Abe, Z. Ogumi, *J. Electrochem. Soc*., **149**, A1578-A1583 (2002).
[68]. Y. M. Lee, J. E. Seo, Y.-G. Lee, S. H. Lee, K. Y. Cho, J.-K. Park, *Electrochem. Solid-State Lett*., **10**, A216-A219 (2007).
[69]. F. Marchioni, K. Star, E. Menke, T. Buffeteau, L. Servant, B. Dunn, F. Wudl, *Langmuir*, **23**, 11597-11602 (2007).
[70]. Y. S. Nimon, M.-Y. Chu, S. J. Visco, Application: US, US 2000-713997 6537701, 2003.
[71]. S. J. Visco, M.-Y. Chu, Application: US, US 98-86665, 6025094, 2000.
[72]. G. B. Appetecchi, F. Croce, L. Persi, F. Ronci, B. Scrosati, *Electrochim. Acta*, **45**, 1481-1490 (2000).
[73]. F. Croce, R. Curini, A. Martinelli, L. Persi, F. Ronci, B. Scrosati, R. Caminiti, J. *Phys. Chem. B*, **103**, 10632-10638 (1999).
[74]. Z. Wen, T. Itoh, M. Ikeda, N. Hirata, M. Kubo, O. Yamamoto, *J. Power Sources*, **90**, 20-26 (2000).
[75]. Z. Wen, T. Itoh, Y. Ichikawa, M. Kubo, O. Yamamoto, *Solid State Ionics*, **134**, 281-289 (2000).
[76]. M. Watanabe, T. Hirakimoto, S. Mutoh, A. Nishimoto, *Solid State Ionics*, **148**, 399-404 (2002).
[77]. R. N. Mason, M. Smith, T. Andrews, D. Teeters, *Solid State Ionics*, **118**, 129-133 (1999).
[78]. S. Gadad, D. Teeters, in *Proceedings, Electrochemical Society*, pp. 288(2001).
[79]. J. L. Koeing, *Spectroscopy of Polymers*. Editor, American Chemical Society, Washington D.C., (1992).
[80]. A. Layson, S. Gadad, D. Teeters, *Electrochim. Acta*, 48, 2207-2213 (2003).
[81]. A. J. Bhattacharyya, J. Fleig, Y. G. Guo, J. Maier, *Advanced Materials*, **17**, 2630-2634 (2005).
[82]. F.M. Gray, *Polymer Electrolytes: RSC materials monographs*, Royal Society of Chemistry, Cambridge (1997), p.31-44.
[83]. H.R. Allcock, S.E. Kuharcik, C.S. Reed, M.E. Napierala, *Macromolecules* **29** (1996) (10) 3384.
[84]. W. Wieczorek, K. Such, H. Wyciślik, J. Płocharski, *Solid State Ionics* **36** (1989) (3-4) 255.

[85]. J. Płocharski, W. Wieczorek, J. Przyłuski, K. Such, *Applied Physics A Solids and Surfaces* **49** (1989) (1) 55.
[86]. J. Przyłuski, K. Such, H. Wyciślik, W. Wieczorek, Z. Floriańczyk, *Synthetic Metals* **35** (1990) (1-2) 241.
[87]. F. Capuano, F. Croce, B. Scrosati, *Journal of the Electrochemical Society* **138** (1991) (7) 1918.
[88]. F. Croce, B. Scrosati, G. Mariotto, *Chemistry of Materials* **4** (1992) (6) 1134.
[89]. N. Munichandraiah, L.G. Scanlon, R.A. Marsh, B. Kumar, A.K. Sircar, *Journal of Applied Electrochemistry* **24** (1994) (10) 1066.
[90]. M.C. Borghini, M. Mastragostino, S. Passerini, B. Scrosati, *Journal of the Electrochemical Society* **142** (1995) (7) 2118.
[91]. W. Wieczorek, K. Such, Z. Florjanczyk, J.R. Stevens, *Journal of Physical Chemistry* **98** (1994) (27) 6840.
[92]. S. Chintapalli, R. Frech, *Solid State Ionics* **86-88** (1996) (PART 1) 341.
[93]. F. Croce, G.B. Appetecchi, L. Persi, B. Scrosati, *Nature* **394** (1998) (6692) 456.
[94]. J.S. Syzdek, M.B. Armand, P. Falkowski, M. Gizowska, M. Karłowicz, Ł. Łukaszuk, M.Ł. Marcinek, A. Zalewska, M. Szafran, C. Masquelier, J.M. Tarascon, W.G. Wieczorek, Z.G. Żukowska, *Chemistry of Materials* **23** (2011) (7) 1785.
[95]. J.B. Goodenough, H.Y.P. Hong, J.A. Kafalas, *Materials Research Bulletin* **11** (1976) (2) 203.
[96]. L. Sebastian, J. Gopalakrishnan, *Journal of Materials Chemistry* **13** (2003) (3) 433.
[97]. J. Płcharski, W. Weiczorek, *Solid State Ionics* **28–30, Part 2** (1988) (0) 979.
[98]. W. Wieczorek, K. Such, H. Wyciślik, J. Płocharski, *Solid State Ionics* **36** (1989) (3–4) 255.
[99]. I. Villarreal, E. Morales, J.L. Acosta, *Die Angewandte Makromolekulare Chemie* **266** (1999) (1) 24.
[100]. H.Y. Sun, Y. Takeda, N. Imanishi, O. Yamamoto, H.-J. Sohn, *Journal of the Electrochemical Society* **147** (2000) (7) 2462.
[101]. C. Capiglia, J. Yang, N. Imanishi, A. Hirano, Y. Takeda, O. Yamamoto, *Solid State Ionics* **154–155** (2002) (0) 7.
[102]. J. Przyłuski, W. Wieczorek, *Solid State Ionics* **36** (1989) (3–4) 165.
[103]. D. Golodnitsky, E. Peled, *Electrochimica Acta* **45** (2000) (8) 1431.
[104]. D. Golodnitsky, E. Livshits, A. Ulus, Z. Barkay, I. Lapides, E. Peled, S.H. Chung, S. Greenbaum, *Journal of Physical Chemistry A* **105** (2001) (44) 10098.
[105]. D. Golodnitsky, E. Livshits, A. Ulus, E. Peled, *Polymers for Advanced Technologies* **13** (2002) (10-12) 683.
[106]. D. Golodnitsky, E. Livshits, R. Kovarsky, E. Peled, S.H. Chung, S. Suarez, S.G. Greenbaum, *Electrochemical and Solid-State Letters* **7** (2004) (11) A412.
[107]. H.V.S.A. Hubbard, S.A. Sills, G.R. Davies, J.E. McIntyre, I.M. Ward, *Electrochimica Acta* **43** (1998) (10-11) 1239.
[108]. R. Kovarsky, D. Golodnitsky, E. Peled, S. Khatun, P.E. Stallworth, S. Greenbaum, A. Greenbaum, *Electrochimica Acta* **57** (2011) (1) 27.
[109]. T.D. Dang, S.J. Bai, D.P. Heberer, F.E. Arnold, R.J. Spry, *Journal of Polymer Science, Part B: Polymer Physics* **31** (1993) (13) 1941.
[110]. Y. Zheng, F. Chia, G. Ungar, P.V. Wright, *Chemical Communications* (2000) (16) 1459.

[111]. Y. Zheng, F. Chia, G. Ungar, T.H. Richardson, P.V. Wright, *Electrochimica Acta* **46** (2001) (10-11) 1397.
[112]. Y. Zheng, F. Chia, G. Ungar, P.V. Wright, *Journal of Power Sources* **97-98** (2001) 641.
[113]. V. Percec, G. Johansson, J. Heck, G. Ungar, S.V. Batty, *Journal of the Chemical Society, Perkin Transactions 1* (1993) (13) 1411.
[114]. G. Ungar, S.V. Batty, V. Percec, J. Heck, G. Johansson, *Advanced Materials for Optics and Electronics* **4** (1994) (4) 303.
[115]. R.A. Vaia, H. Ishii, E.P. Giannelis, *Chemistry of Materials* **5** (1993) (12) 1694.
[116]. R.A. Vaia, K.D. Jandt, E.J. Kramer, E.P. Giannelis, *Macromolecules* **28** (1995) (24) 8080.
[117]. J. Syzdek, M. Armand, M. Gizowska, M. Marcinek, E. Sasim, M. Szafran, W. Wieczorek, *Journal of Power Sources* **194** (2009) (1) 66.
[118]. J. Syzdek, M. Armand, M. Marcinek, A. Zalewska, G. Zukowska, W. Wieczorek, *Electrochimica Acta* **55** (2010) (4) 1314.
[119]. M. Volel, M. Armand, W. Gorecki, M.L. Saboungi, *Chemistry of Materials* **17** (2005) (8) 2028.
[120]. M. Riley, P.S. Fedkiw, S.A. Khan, *Journal of the Electrochemical Society* **149** (2002) (6) A667.
[121]. M.W. Riley, P.S. Fedkiw, S.A. Khan, *Journal of the Electrochemical Society* **150** (2003) (7) A933.
[122]. G. Sandí, R. Kizilel, K.A. Carrado, R. Fernández-Saavedra, N. Castagnola, *Electrochimica Acta* **50** (2005) (19) 3891.
[123]. L.J. Lee, C. Zeng, X. Cao, X. Han, J. Shen, G. Xu, *Composites Science and Technology* **65** (2005) (15-16 SPEC. ISS.) 2344.
[124]. M.L.K. Hoa, M. Lu, Y. Zhang, *Advances in Colloid and Interface Science* **121** (2006) (1-3) 9.
[125]. N.T. Kalyana Sundaram, T. Vasudevan, A. Subramania, *Journal of Physics and Chemistry of Solids* **68** (2007) (2) 264.
[126]. H. Chen, G.R. Palmese, Y.A. Elabd, *Chemistry of Materials* **18** (2006) (20) 4875.
[127]. C. Bishop, D. Teeters, *Electrochimica Acta* **54** (2009) (16) 4084.
[128]. M. Castriota, D. Teeters, *Ionics* **11** (2005) (3-4) 220.
[129]. P. Hari, M. Byrczek, D. Teeters, P. Utekar, *International Journal of Nanoscience* **10** (2011) (1-2) 81.
[130]. A.R. Layson, D. Teeters, *Solid State Ionics* **175** (2004) (1-4) 773.
[131]. S. Vorrey, D. Teeters, *Electrochimica Acta* **48** (2003) (14-16 SPEC.) 2137.
[132]. A. Schönhals, H. Goering, C. Schick, *Journal of Non-Crystalline Solids* **305** (2002) (1-3) 140.
[133]. K. Lagrené, J.M. Zanotti, *European Physical Journal: Special Topics* **141** (2007) (1) 261.
[134]. V.A.E.V.M. Bershtein, *Differential scanning calorimetry of polymers : physics, chemistry, analysis, technology*, Ellis Horwood, New York (1994).
[135]. B.A. Wunderlich, *Macromolecular physics 3, Crystal melting*, Academic press, New York [etc.] (1980).
[136]. H. Schönherr, C.W. Frank, *Macromolecules* **36** (2003) (4) 1199.
[137]. L. Gitelman, M. Israeli, A. Averbuch, M. Nathan, Z. Schuss, D. Golodnitsky, *Journal of Computational Physics* **227** (2008) (18) 8437.